

Elaborating the connections of a closed-loop forebrain circuit in the rat: Circumscribed evidence for novel topography within a cortico-striato-pallidal triple descending projection, with thalamic feedback, to the anterior lateral hypothalamic area

Kenichiro Negishi^{1-4,7,8+*}, Vanessa I. Navarro^{1-5,7+}, Laura P. Montes¹⁻⁴, Lidice Soto Arzate^{1,6,7}, Josedell M. Guerra Ruiz^{1,7}, Diana Sotelo^{1,2,5,7}, Alejandro R. Toccoli^{1,2,5,7} and Arshad M. Khan^{1-7*}

¹UTEP Systems Neuroscience Laboratory, ²Department of Biological Sciences, ³Border Biomedical Research Center, ⁴PhD Program in Bioscience, ⁵UTEP RISE Program, ⁶UTEP LSAMP PRELS Program, ⁷HHMI PERSIST Brain Mapping & Connectomics Undergraduate Teaching Laboratory, The University of Texas at El Paso, El Paso, TX 79968.

⁸Present address: Behavioral Neuroscience Branch, IRP/NIDA/NIH, Baltimore, MD.

⁺*co-first authors*

**Address correspondence to:*

Arshad M. Khan, Ph.D. (amkhan2 [at] utep.edu) and
Kenichiro Negishi, Ph.D. (ken.negishi [at] nih.gov)

Key words

nucleus accumbens, ventral pallidum, substantia innominata, lateral hypothalamic area, paraventricular nucleus, prefrontal cortex, amygdala, hippocampus, anterograde, retrograde, connections, motivation, reward, atlas

Abstract

Motivated behaviors are regulated by distributed forebrain networks. Traditional approaches have often focused on individual brain regions and connections that do not capture the topographic organization of forebrain connectivity. We performed co-injections of anterograde and retrograde tract tracers in rats to provide novel high-spatial resolution evidence of topographic connections that elaborate a previously identified closed-loop forebrain circuit implicated in affective and motivational processes. The nodes of this circuit include select regions of the medial prefrontal cortex (defined here more specifically as the cingulate region, CNG), a dorsomedial portion of the nucleus accumbens (ACBdm), a portion of the medial substantia innominata (SIm), and the anterior lateral hypothalamic area (LHAa). The circuit also reportedly receives a feedback loop from the anterior region of the paraventricular thalamic nucleus (PVTa). In this draft report, we provide detailed circumscribed evidence supporting these regions as interconnected nodes, and provide several novel findings concerning the topographic organization of their projections. First, we identified the ACBdm based on its unique connectivity. Anterograde labeling from anterior paraventricular thalamic nucleus (PVTa) and retrograde labeling from medial substantia innominata (SIm) and lateral hypothalamic area (LHA) were restricted to the dorsomedial ACB (ACBdm). Strikingly, this labeling formed a longitudinal column extending along virtually the entire anteroposterior axis of ACBdm. Subsequent analysis revealed a convergence of ACBdm axon terminals and retrogradely labeled neurons from LHA within the anterior SIm. Furthermore, we identified cortical CNG regions related to this circuit. These regions contained retrograde labeling from both ACBdm and LHA, and anterograde labeling from PVTa. These cortical subdomains included regions previously implicated in the circuit but for which detailed organization has been unknown: (1) a region between the posterior prelimbic and infralimbic areas; (2) posterior part of basolateral and basomedial amygdalar nuclei, and (3) anterior pole of ventral subiculum. Our circumscribed findings, which await additional samples and analysis, support the existence of a topographically organized closed-loop circuit and identify two additional novel features: (1) direct evidence for an elaborate *core rostrocaudal topography* for a cortico–striato–pallidal motif comprising a triple descending projection to the LHA via direct, indirect, and “hyperdirect” pathways, and (2) a thalamic feedback system with specific projections to *each cortical and striatal node* of the circuit. We discuss the implications of this newly elaborated circuit for understanding the neural basis of motivational processes.

Significance Statement

We used a bottom-up approach to identify a distinct longitudinal column of dorsomedial nucleus accumbens (ACBdm) that spans its anteroposterior axis. This region projects to medial substantia innominata (SIm) and lateral hypothalamic area (LHA), resembling the “direct” and “indirect” pathways of the classical basal ganglia circuit. We also identified topographically distinct regions in medial prefrontal cortex (strictly delineated here as the cingulate region, CNG), ventral subiculum (SUBv), and basolateral amygdala (BLA) that project to both ACBdm and LHA, further defining the circuit. Finally, we identified an LHA-to-anterior paraventricular thalamic nucleus (PVTa) feedback projection that selectively targets cortical and striatal nodes within the circuit. Our work provides novel detailed maps that bolster the proposal that this “triple descending projection” (cortico-striato-pallidal) and associated thalamic feedback loop play a role in affective and motivational processes.

1: Introduction

Motivated behaviors unfold as discrete and unitary sets of actions with clear goals and phases (i.e. initiation, consummation, termination) (Watts & Swanson, 2002; Watts et al., 2022). Cerebral hemisphere connections allow integration of internal and external sensory information to adaptively control motivated behaviors, but a structural framework for cerebral hemisphere connections has yet to be established. One prevalent model of cerebral hemisphere connections is the well-studied basal ganglia ‘motor circuit’ (Alexander et al., 1986). This circuit joins cortex, striatum, pallidum, midbrain, and thalamus in anatomically and functionally segregated feedforward loops. Moreover, recent work revealed that basal ganglia circuits are topographically organized into non-overlapping and parallel subregional domains at every division of the circuit (Foster et al., 2021; Lee et al., 2020). Most models, however, do not include the hypothalamus.

In one meticulous synthesis, the basal ganglia circuit architecture was proposed to generalize to hypothalamic systems that control motivated behaviors (Swanson, 2000), but this possibility has not been systematically explored to date at the high-spatial resolution provided by the standardized atlas mapping of circuits. There are indications that some basal ganglia circuit motifs can be identified in regions connected with the lateral hypothalamic area (LHA). In particular, one study described a basal ganglia-like circuit in which the infralimbic area (ILA), a dorsomedial subdomain of the ACB (ACBdm), a medial aspect of substantia innominata (SIm; alternatively, the ventral pallidum), LHA anterior group (LHAa), and paraventricular thalamic nucleus (PVT) formed a topographically organized closed-loop circuit (Thompson & Swanson, 2010). We reasoned that if these regions are components of a basal ganglia circuit, we can predict the existence of a triple descending projection (Swanson, 2000) consisting of ‘hyperdirect’, ‘direct’, and ‘indirect’ pathways that are associated with basal ganglia circuits. We can also expect the triple descending projection to be segregated from adjacent basal ganglia circuits.

Our goal, therefore, was to determine whether the ACBdm-centered circuit described by Thompson & Swanson (2010) exhibits the topographic organization, Swanson’s proposed triple descending projection, and the reported closed-loop architecture that characterizes the basal ganglia circuit. The existence of such features would provide further support that basal ganglia circuit motifs could be the general architecture of the cerebral hemispheres, as has been proposed (Swanson, 2000). Our work was also motivated by the consistent identification of a transcriptionally unique striatal neuron population, referred to as D1/D2 hybrid or ‘eccentric’ neurons, which are enriched in ACBdm (Gagnon et al., 2017). Additionally, a recent study of striatal neuropeptides found enriched expression of the striosomal marker prepronociceptin in ACBdm (Hueske et al., 2024). Thus, the ACBdm appears to be distinguishable from other striatal and ACB regions with respect to connectivity, gene expression, and neuropeptide content. Further exploration of the ACBdm will likely yield insights into cerebral hemisphere functions.

Although basal ganglia circuits are diagrammatically simple, their topographic organization makes them challenging to delineate anatomically. Basal ganglia circuit anatomy is often studied using a top-down approach. In this approach, tracer injections into cortical or striatal areas are treated as experimental starting points from which the basal ganglia circuits are traced (Foster et al., 2021; Hintiryan et al., 2016; Lee et al., 2020). Top-down approaches capture many aspects of corticostriatal and striatopallidal projections with topographic precision, but they can also limit the set of considered regions. In contrast, a bottom-up approach is useful for identifying the full range of areas to be considered for a basal ganglia circuit, and they can be used to clarify the three-

dimensional shapes of distinct connectional domains, where they exist. Bottom-up approaches take advantage of the relative simplicity of striatopallidal and striatohypothalamic projections (Heimer et al., 1991; Zahm & Heimer, 1993) compared to the more dispersed corticostriatal axons (Berendse et al., 1992; Vertes, 2004). Top-down and bottom-up approaches are mutually informative and can eventually lead to clarified circuit maps.

Here we used co-injections of anterograde (*Phaseolus vulgaris* leucoagglutinin; PHAL) (Gerfen & Sawchenko, 1984) and retrograde (cholera toxin B subunit; CTB) (Luppi et al., 1990) tracers to further characterize the circuit formed by ACBdm connections. The ACBdm is known to receive a discrete projection from PVT and in turn send projections to the LHAA and an anteromedial aspect of SI (Thompson & Swanson, 2010). We first used retrograde tracer injections in PVT, SIm, and LHAA to determine the spatial extent of the ACBdm. Next, we used anterograde tracer injections in ACBdm and retrograde labeling from LHAA to confirm that ACBdm projections to SIm are restricted to a small subdomain that projects strongly to LHAA. These observations describe a basal ganglia circuit motif formed around ACBdm connections. Finally, we determined the cortical components of this circuit by identifying areas that received inputs from PVT and project to both ACBdm and LHAA. Taken together, we present evidence, portions of which have been reported in conference presentations (Guerra Ruiz et al., 2021; Negishi et al., 2022; 2023; Soto Arzate et al., 2023), for a forebrain closed-loop circuit that consists of a descending cortical–striatal–pallidal triple projection to LHA and a thalamic feedback system that projects to the cortical components and ACBdm. We discuss some implications of these circuit motifs and the parallel and segregated loop architecture in the context of affective and motivational processes.

2: Materials and Methods

2.1: Naming conventions

For all our anatomy, we used the spatial framework, nomenclature system and ontology of Swanson (2015; 2018). Specifically, this report contains data populating brain regions named in accordance with Swanson (2015), as applied to the rat brain in *Brain Maps 4.0*, an open-access rat brain atlas (Swanson, 2018), and includes standard terms. Each standard term is set in italics and includes the named neuroanatomical structure and the associated (author, date) citation that first uses the term as defined, e.g., “*lateral hypothalamic area (Nissl, 1913)*”. For those terms where assignment of priority was not possible, they are assigned the annotation “(>1840)”, i.e., “defined sometime after the year 1840”, a year which roughly marks the introduction of cell theory in biology, e.g., “*dorsomedial hypothalamic nucleus (>1840)*”. Standard terms for *gray matter regions* (Swanson & Bota, 2010) can be found in “Table C: Rat CNS Gray Matter Regions 4.0 (Topographical Histological Groupings)” from the Supporting Information available online for Swanson (2018), which is based on the scientific literature and cytoarchitectonic features of Nissl-stained tissue sections. Similarly, *white matter tracts* (Bell & Bell, 1826) are listed in “Table D: Rat CNS White Matter Tracts 4.0 (Topographic Histological Groupings)” from the same Supporting Information, e.g., “*hypothalamic postcommissural fornix (Swanson, 2015)*”. Importantly, any citation included within the standard term is included in the list of cited references in this study. A list of the standard terms and the abbreviations used in this study is provided in the Abbreviations section. In this study, we additionally employ the abbreviations “ACBdm”, “PVTa”, and “SI_m”, which are not formally present in Swanson (2018) but which informally name subregions following the abbreviation system of Swanson (2018) and also elaborated in Thompson & Swanson (2010). Further discussion will be needed to formally include or refine these subregions in future versions of the atlas.

2.2: Subjects

Currently, this report draft documents patterns of connectivity from four adult male rats (Envigo), who were maintained on a 12 h:12 h light/dark cycle (lights off at 6:00 pm) with ad libitum access to food and water. Patterns from experiments on additional male rats (n=10) and a cohort of female rats (n=17) await full analysis, the sample sizes for which are also parsed below by region. We housed two rats per cage prior to surgery and individually after surgery. We performed the experiment on the subjects reported here in accordance with the *NIH Guide for the Care and Use of Laboratory Animals* (8th edition), under protocol A-202203-1, approved by the Institutional Animal Care and Use Committee at the University of Texas at El Paso.

2.3: Tracers and injection site definitions

We used the iontophoresis method for PHAL and CTB co-injections, as described previously (Negishi et al., 2024). Glass micropipettes (tip diameters: 12–20 μm) were filled with a cocktail containing 2.5% PHAL (Vector Laboratories, Inc., Newark, California, USA; catalog #L-1110) and 0.25% CTB (List Biological Labs, Inc., Campbell, California, USA; catalog #104) dissolved in 10 mM sodium phosphate solution. Injection sites for immunodetected PHAL were determined by examining the distributions of labeled neurons. This follows from the recognition that PHAL uptake occurs in dendrites and must label the soma before continuing into axons. For CTB, immunolabel or fluorescence can clearly demarcate the limits of injection spread. CTB is

primarily used as a retrograde tracer, but it is also known to have some weak anterograde transport that can be observed at the injection site. We defined CTB injection spread based on areas that contained dense labeling that was not only due to labeled processes.

In discussing the spatial locations of injections and labeled tracers, we adopt the notation $^{SW}AP^{\beta}$, where β denotes the approximate anterior-posterior distance (in mm from Bregma) and SW indicates the corresponding atlas level (L) from Swanson (1992, 1998, 2004; 2018). We used Nissl-defined boundaries to locate the injections within the atlas framework of BM4. As such, all our stereotaxic information is based on first-order approximations by Swanson.

2.4: Intracranial surgeries and tracer injections

We anesthetized the rats and maintained them under isoflurane (5% induction, 2–3% maintenance, Covetrus). Rats were head-fixed on a stereotaxic instrument (Kopf), and midline incisions were made to prepare the scalp prior to craniotomy. We carefully exposed the surface of the dura mater with a round head drill and a bent syringe tip was used to remove dura at the brain entry site. For iontophoresis, we loaded tracers into glass micropipettes and lowered them into brain targets based on coordinates from Paxinos and Watson (2014). We used either a BAB-600 (M1160; Kation Scientific) or Midgard current source (Stoelting) to deliver 5 μ A in 7 s ON/OFF cycles over 15–30 min. Pipettes were removed after a 10-min diffusion period. Rats received iontophoretic injections of the tracers in the ACBdm (n = 11; AP: +1.6 mm, ML: \pm 0.8 mm, DV: –5.20 mm from dura), SIm (n = 7; AP: 0.0 mm, ML: \pm 1.50 mm, DV: –7.1 mm from dura), LHAA (n = 8; AP: –1.7 mm, ML: \pm 2.0 mm, DV: –8.1 mm), and PVT (n = 5; AP: –1.5 mm, ML: \pm 1.0 mm (angled 10° inward), DV: –4.7 mm from dura). Under our approved protocol, care is taken to provide post-surgical care in the form of analgesia (Flunazine; Bimeda-MTC Animal Health, Inc., catalog #200-387) and also antibiotics (Gentamicin; Vedco, Inc., St. Joseph, Missouri, USA; catalog #50989-040-12) as necessary. Animals are monitored for adverse signs throughout the survival period for tracer transport (10–14 d).

2.4: Tissue preparation

After surgery, we maintained the rats for a 7- to 10-day survival period before euthanasia. We deeply anesthetized rats with isoflurane saturated in an enclosed glass desiccator bell jar for 70 s and perfused them transcardially with 200 ml of PBS, pH 7.4, followed by paraformaldehyde (PFA), freshly depolymerized to a 4% solution in phosphate-buffered saline (PBS). We removed the brains and placed them into the PFA solution for post-fixation overnight in 4°C. We transferred the brains to PBS containing 30% sucrose on the following day.

We froze PHAL and CTB co-injected brains on a sliding microtome stage (Leica Microsystems) with dry ice. We collected 30- μ m coronal sections into 24-well plates divided into 6 series and stored sections in cryoprotectant (50% phosphate buffer, 20% glycerol, and 30% ethylene glycol) and at –20°C until further processing. For brains injected with fluorescent CTB, we froze the brains in dry ice and sectioned them in a cryostat (Leica Microsystems). We collected coronal sections of 40- μ m thickness into four series and stored them in cryoprotectant at –80°C.

2.5: Immunohistochemistry

To single-label PHAL and CTB, we used immunoperoxidase staining based on our previous work (Bono et al., 2024; Negishi et al., 2024). We removed tissues from cryoprotectant and washed them in 0.05 M Tris-buffered saline (TBS; pH 7.4 at room temperature) for five

washes, each for five min (5×5). We treated sections with 0.014% phenylhydrazine for 20 min to suppress endogenous peroxidase activity. After another 5×5 wash, we incubated tissues for 2 h in a blocking solution containing 2% (v/v) normal donkey serum (EMD Millipore; Catalog #S30) and 0.1% Triton X-100 (Sigma-Aldrich; Catalog #T8532). We then incubated tissues in primary antiserum containing antibodies raised against PHAL (host: rabbit; dilution: 1:4,000; Vector Labs, Cat # AS-2224; RRID: AB_2313686) or CTB (host: goat; dilution: 1:10,000; List Biological Cat # 703; RRID: AB_10013220) in blocking solution for 48 h in 4°C. After a 5×5 TBS wash, we incubated the sections in secondary antiserum with biotinylated antibodies raised against rabbit (host: donkey; dilution: 1:1,000; Jackson ImmunoResearch Labs, Cat# 711-065-152; RRID: AB_2340593) or goat (host: donkey; dilution: 1:1,000; Jackson ImmunoResearch Labs, Cat# 705-065-147; RRID: AB_2340397) for 5 h followed by another 5×5 TBS wash. Next, we amplified signal via formation of avidin-biotin-horseradish peroxidase complexes (Vectastain ABC HRP Kit, Vector, 45 μ l reagent A and B per 10 ml) in 0.05 M TBS containing 0.1% Triton X-100 (v/v) for 1 h. We rinsed tissues and developed them in 0.05% 3, 3'-diaminobenzidine (DAB) (Sigma-Aldrich) mixed with 0.015% H₂O₂ in 0.05 M TBS for 10–20 min for PHAL. For CTB, we developed sections with heavy metal intensification by mixing 0.05% DAB with 0.005% H₂O₂, 0.1% ammonium nickel (II) sulfate in 0.05 M TBS. Sections were then washed in TBS (5×5), mounted onto gelatin-coated slides, and left to dry overnight at room temperature. Finally, tissue sections were dehydrated with ascending concentrations of ethanol (50–100%), defatted in xylene, and coverslipped with DPX mounting medium (Cat # 06522; Sigma-Aldrich).

For immunofluorescent labeling for PHAL and CTB, we washed tissues in TBS (5×5), transferred them into blocking solution, and then incubated them in primary antiserum following the same parameters as above. We prepared primary antiserum with antibodies raised against PHAL and CTB. After tissues were washed in TBS (5×5), we transferred them into secondary antiserum containing biotinylated antibodies raised against rabbit and Cy3-conjugated antibodies against goat (host: donkey; dilution: 1:1,000; Jackson ImmunoResearch Labs, Cat# 705-165-147; RRID: AB_2307351) for 5 h. Following another wash, we reacted tissues with Alexa Fluor 488-conjugated streptavidin (dilution: 1:1,000; ThermoFisher Scientific, Cat# S11223) and NeuroTrace 660/640 (dilution: 1:200; ThermoFisher Scientific, Cat# N21483) for 1 h. After a final wash in TBS, we mounted the free-floating sections onto glass slides and left them to dry. We coverslipped tissues using sodium bicarbonate-buffered glycerol (pH 8.4 at room temperature) and sealed them with nail polish.

2.6: Antibody validation

Antisera for this study only contained antibodies raised against PHAL and CTB. Specific staining was not observed for PHAL or CTB in rats that did not receive tracer co-injections. Additionally, specific staining was not evident for injection cases that did not effectively transport tracers. The same validation approach and outcome were found in other reports that cataloged the same antibodies (Hahn & Swanson, 2010, 2012). Specificity for secondary antibodies was determined with no-primary controls. The immunohistochemistry procedures were performed as described but with the omission of primary antibodies in the first antiserum. No labeling was detectable for the secondary antibodies we used in the absence of the primary antibody.

2.7: Nissl staining

Sections were first washed (5×5) in 0.05 M TBS (pH 7.4 at room temperature) to remove

cryoprotectant. Free-floating sections were mounted onto gelatin-coated glass slides and dried overnight at room temperature. Sections were dehydrated through ascending concentrations of ethanol (50%, 70%, 95%, and 100%) and defatted in xylenes for 25 min. Next, they were rehydrated and stained with a 0.25% thionine solution (thionin acetate, Catalog #T7029; Sigma-Aldrich Corporation, St. Louis, MO) and differentiated in 0.4% anhydrous glacial acetic acid. Stained slides were dehydrated again and coverslipped with DPX mounting medium and left to dry overnight.

2.8: *Microscopy*

Immunostained and Nissl-stained sections were visualized and photographed under brightfield and darkfield microscopy using a BX63 microscope (Olympus Corporation, Shinjuku, Japan) equipped with a DP74 color CMOS camera (cooled, 20.8 MP pixel-shift, 60 fps). Image acquisition with a $\times 10$ objective (N.A. 0.4), stitching (15% image overlap), and .TIFF image exporting were performed with cellSens Dimension™ software (Version 2.3; Olympus Corporation). Images were adjusted for brightness and contrast using Adobe Photoshop (Version 13.0.1; Adobe Systems, Inc) and exported to Adobe Illustrator (*Ai*; Version CC 18.0.0; Adobe Systems, Inc.) for parcellation. Images were adjusted for brightness and contrast using Adobe Photoshop and exported to *Ai* for parcellation.

For immunofluorescence imaging, we used an Olympus VS200 Slide Scanner. We obtained four-channel mosaic images using $\times 10$ objectives for each section and then exported channels separately as grayscale 16-bit .PNG files. We then applied linear scaling to produce 8-bit images with upper and lower bounds based on their intensity histograms.

2.9: *Mapping of immunohistochemically detected tracers*

The atlas-based mapping approach used here follows the cytoarchitectonic approach described by Swanson (1992, 1998, 2004; 2018). Briefly, formal cytoarchitecture-based definitions and nomenclature for gray matter regions were obtained for all areas examined (see Table C in Supplementary Information Folder 1 from Swanson [2018]), boundaries were drawn with Nissl-stained reference sections and then superimposed on images of labeled tracers for localization. Serial collection and staining allowed for each tracer-labeled section to have an adjacent Nissl-stained section for reference. We placed images of Nissl- and immuno-stained tissues onto *Ai* files as separate layers and aligned them based on shared features (i.e., brain surfaces, white matter tracts, background staining, and blood vessels). We drew Nissl-based boundaries on a separate layer, and these were used to determine the correct locations of tracer distributions. We then transformed the raw data into segmentation masks and manually registered them to standard atlas plates from *Brain Maps 4.0* (BM4; Swanson, 2018). It should be emphasized that the transcription process, in our case, was a representation and never an attempt to simply fit or copy-paste information. Matching histological sections to atlas levels involved careful scrutiny of the histological plane-of-section and other forms of non-linear distortion (Simmons & Swanson, 2009). Once the corresponding atlas levels were identified, we created maps using data from only the best-matched sections. We aimed to accurately show spatial information with an attempt to also capture some morphological features such as connective density, direction, and axonal morphology.

3: Results

3.1: Injection sites

We selected injection experiments from four male subjects to display patterns of topographic organization in this report. Additional data are being collected from 27 male and female rats, so at the time of this writing, the data presented here are circumscribed. The experiments described below follow from PHAL and CTB co-injections targeting dmACB, LHAA, and PVTa (**Figure 1**). Experiment #19-059 is centered in the ACBdm in $L^{13}AP^{\beta+1.5}$ for both PHAL and CTB (**Figure 1**). The CTB in this experiment appears to have spread more than PHAL. Importantly, both injections remain within the boundaries of ACB and are concentrated within its dorsomedial tip. Experiment #19-011 is centered in an anterior part of PVT at $L^{25}AP^{\beta-1.5}$ based on the shape and size of the paratenial (PT), mediodorsal (MD), and central medial (CM) thalamic nuclei. The injection is largely restricted to one hemisphere, and there appears to be slight spillover into the neighboring MD. The injection site for experiment #19-056 is restricted to the LHAA. In this group, CTB is centered in the ventral zone and shows some spillover into the intermediate zone dorsally. PHAL is only found in the ventral zone of LHAA. The cytoarchitecture of paraventricular (PVH) and anterior (AHN) hypothalamic nuclei suggest this injection is at $L^{25}AP^{\beta-1.5}$. Based on its location

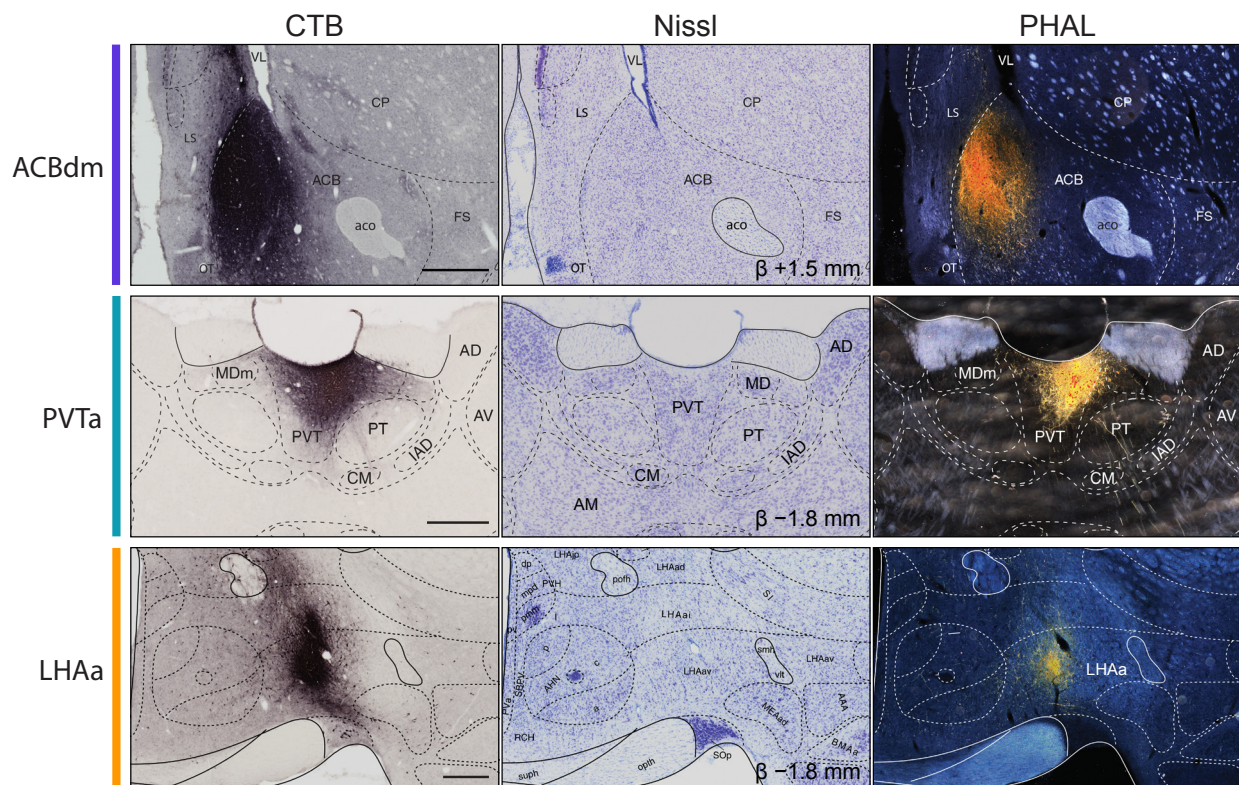


Figure 1. Histological localization of co-injected anterograde and retrograde tracers. Photomicrographs showing immunodetected PHAL (*left column*), CTB (*right column*), and their corresponding Nissl-stained sections (*middle column*). (**Top row**) Representative injection site in ACBdm at approximately +1.5 mm from bregma. (**Middle row**) Representative injection site in PVTa at approximately -1.8 mm from bregma. (**Bottom row**) Representative injection site in LHAA at approximately -1.8 mm from bregma. Superimposed boundaries are based on the cytoarchitecture shown in the Nissl-stained sections. See Abbreviations for nomenclature. Scale bars: 500 μ m.

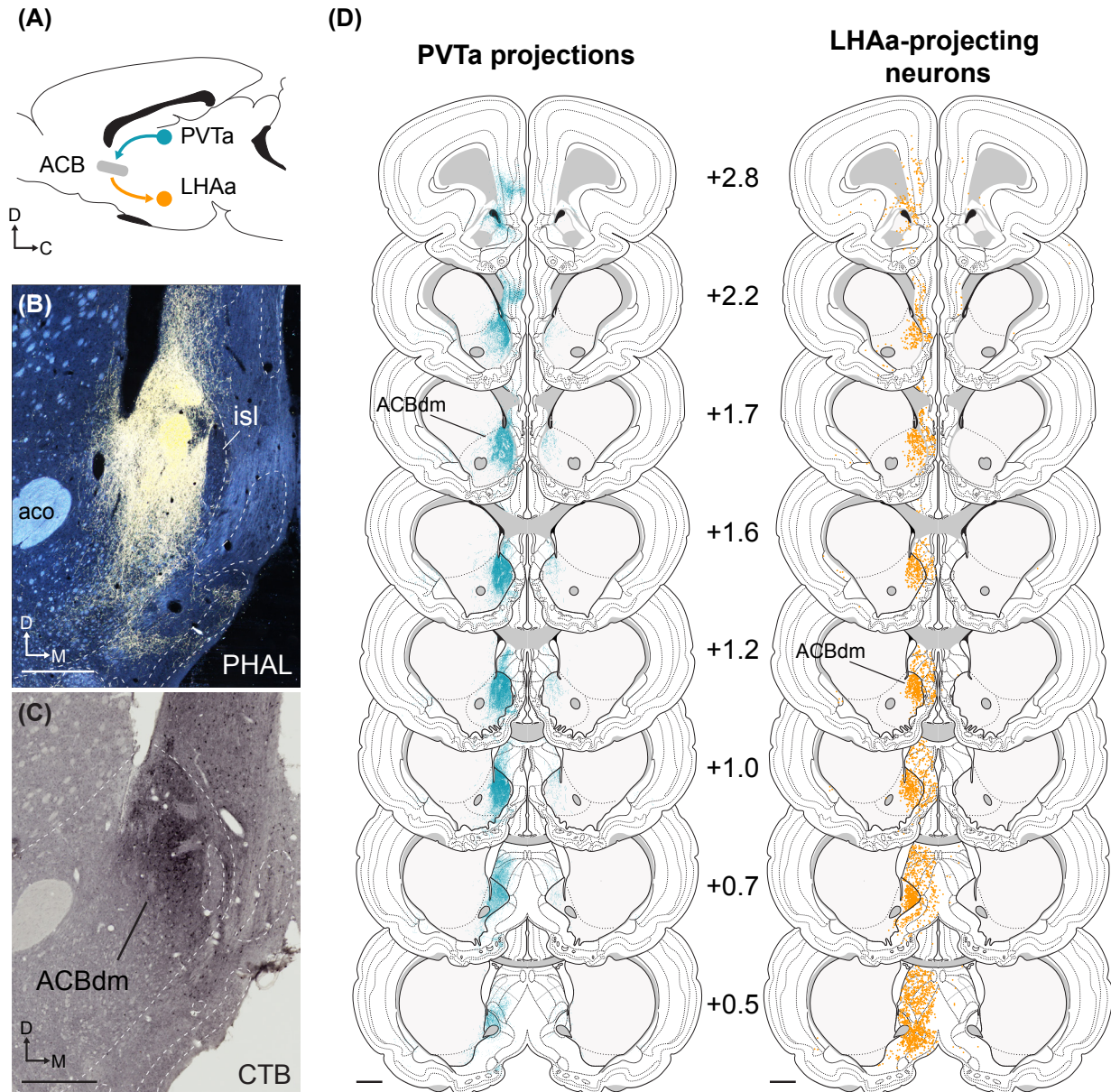


Figure 2. Convergent PVTa and LHAA connections in ACBdm. **(A)** Diagrammatic representation of experiments. **(B)** Darkfield photomicrograph showing PHAL-labeled axons in ACBdm following an injection into PVTa. **(C)** Brightfield photomicrograph showing CTB-labeled neurons in ACBdm following an injection into LHAA. Boundaries shown in **(B)** and **(C)** were determined using adjacent Nissl-stained sections. **(D)** Mapped distributions of PVTa axons (*green*) and LHAA-projecting neurons (*orange*) across the anterior-posterior span of ACB. The caudoputamen and ACB are indicated using solid boundaries and gray shading. Values in the middle denote approximate distance from bregma. See Abbreviations for nomenclature. Scale bars: 500 μ m (**B**, **C**), 1 mm (**D**).

in the LHAA ventral zone, this injection may also overlap with the retinorecipient zone of LHAA (Canteras et al., 2011).

3.2: An ACBdm subregion defined by bottom-up PVTa and LHAA connections

We first examined the connections of LHAA, and PVTa to identify zones of overlap. We used Nissl-based mapping to achieve spatial normalization within the atlas framework of BM4. This allowed us to compare distributions of PHAL and CTB from the PVTa and LHAA (Fig. 2A). Our co-injection experiments suggest showed that PVTa formed dense PHAL-labeling in the ACBdm whereas no CTB was detected (Fig. 2B). LHAA co-injection, in contrast, predominantly labeled ACBdm with CTB (Fig. 2C). PHAL and CTB from PVTa and LHAA showed remarkably strong overlap within the ACBdm. Therefore, we next determined the anterior-posterior limits of overlap. Unexpectedly, this connectional overlap spanned the entire anterior-posterior extent of ACB, forming a 2-mm longitudinal column in its dorsomedial aspect at $L9-16AP^{\beta+0.5}$ to $+2.80$ (Fig. 2D). Closer examination of Nissl architecture and tracer distributions suggests some compartmental specificity. Labeling from PVTa, LHAA was absent in the major island of Calleja (isl) medially. Note that labeling in ACBdm was lighter in narrow strips that are reminiscent of striosomes (alternatively, striatal patches). Importantly, labeling from the regions was virtually absent in the rest of caudoputamen (CP), other ACB, or striatal fundus (SF). We can note additional overlap between PVTa and LHAA in a ventrolateral aspect of lateral septum (LS).

3.3: A striatopallidal 'indirect' pathway from ACBdm

Others have described a striatopallidal intermediate pathway connecting ACBdm to LHAA through SIm (Thompson & Swanson, 2010), but their zone of overlap remains unclear. We sought to examine the distributions of PHAL transport from a rostral part of ACBdm and CTB-immunoreactive neurons retrogradely labeled from the LHAA (Fig. 3A). In SI, ACBdm axon terminals formed a dense cluster within a roughly 0.1 mm^3 volume of SIm just below the anterior commissure at $L16-18AP^{\beta-0.15}$ to $+0.11$. Retrograde labeling from the LHAA was concentrated in

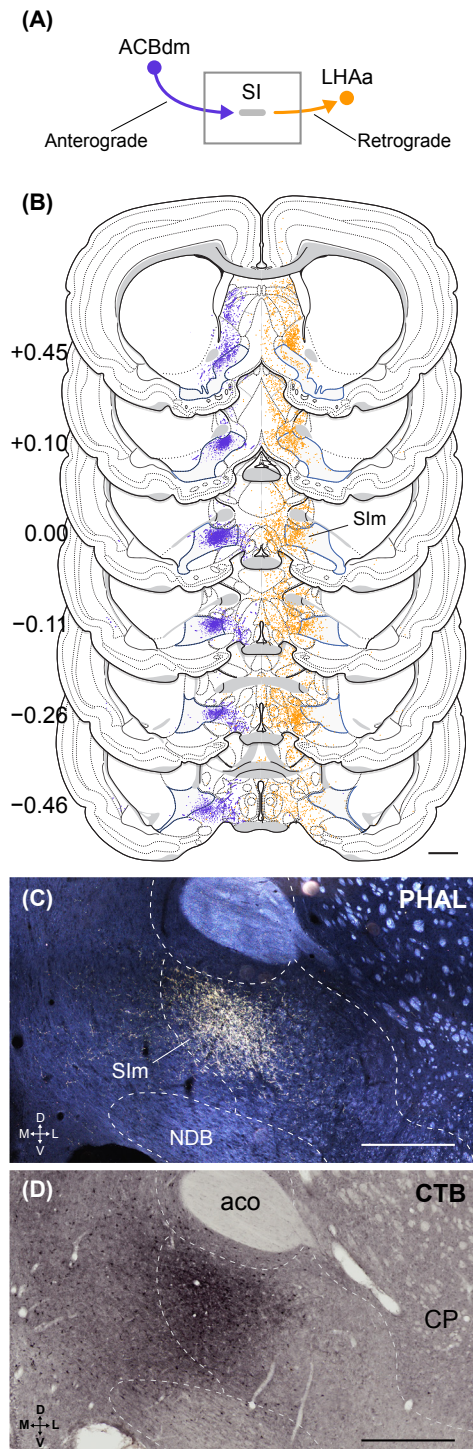


Figure 3 (above). Convergent ACBdm and LHAA connections in SIm. (A) Diagrammatic representation of experiments. (B) Mapped distributions of ACBdm axons (purple) and LHAA-projecting neurons (orange) in an anterior part of SIm. SI is shaded in gray and is bounded with blue outlines. Experimental results are shown in opposite hemispheres for clarity. (C) Darkfield photomicrograph showing ACBdm axon terminals in SIm. (D) Brightfield photomicrograph showing CTB-labeled neurons in SIm after an injection into LHAA. Boundaries were determined using adjacent Nissl-stained sections. See Abbreviations for nomenclature. Scale bars: 1 mm (B), 500 μm (C, D).

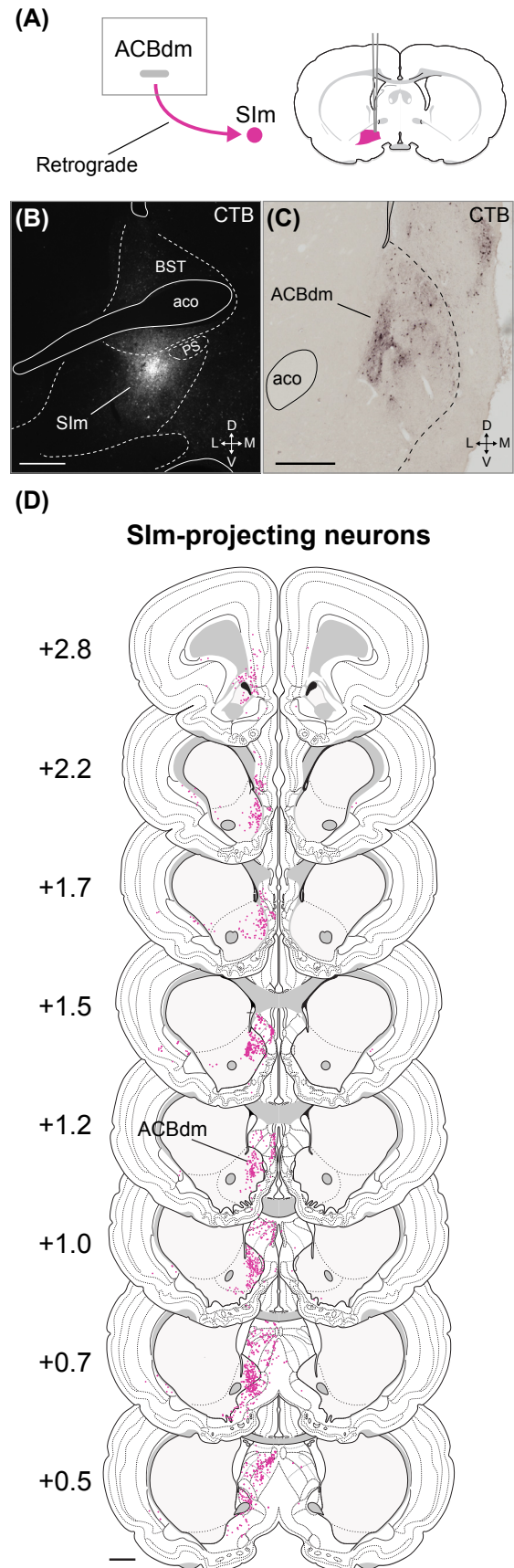
the part of SI that received the ACBdm projection (**Fig. 3B**). The ACBdm terminal in SIm is the densest we observed among any of its connections. Note that PHAL labeling from ACBdm is highly restricted to the same subcommissural space that is concentrated with CTB labeling from LHAA (**Fig. 3C, D**). SI volumes outside this zone of overlap were sparsely connected with ACBdm or LHAA if labeling was detected at all.

We identified a zone of overlapping ACBdm and LHAA connections in the ACBdm, but it remained unclear whether this anterior space of SIm received projections from other parts of the striatum. We determined the striatal distributions of SIm using PHAL and CTB co-injections into this region (**Fig. 4A**). A small injection from experiment #23-024 was centered in the subcommissural SIm at $L^{18}AP^{\beta+0.11}$ based on the cytoarchitecture of the bed nuclei of the stria terminalis and the position of the anterior commissure (**Fig. 4B**). In striatum, this injection produced strong retrograde labeling in the ACBdm that appeared to avoid striosome-like spaces (**Fig. 4C**). CTB labeling from SIm was restricted to the ACBdm column as observed for PVTa and LHAA connections through out $L^{9-16}AP^{\beta+0.5}$ to $+2.80$ (**Fig. 4D**). In contrast to PVTa and LHAA, SIm labeling in LS was more prominent in dorsomedial parts.

3.4: Cortical connections with the ACBdm circuit

Our bottom-up tracing strategy identified a topographically organized basal ganglia-like circuit motif centered around the ACBdm. To this point, we described striatopallidal connections that

Figure 4 (right). Retrograde labeling from SIm is restricted to ACBdm. **(A)** Diagrammatic representation of experiments. **(B)** Fluorescence photomicrograph showing CTB injection site in SIm. **(C)** Brightfield photomicrograph showing immunodetected CTB in ACBdm following an injection in SIm. Boundaries were determined using adjacent Nissl-stained sections. **(D)** Mapped distributions of CTB-labeled neurons (purple dots) in ACB following an injection in SIm. See Abbreviations for nomenclature. Scale bars: 500 μ m (**B, C**), 1 mm (**D**).



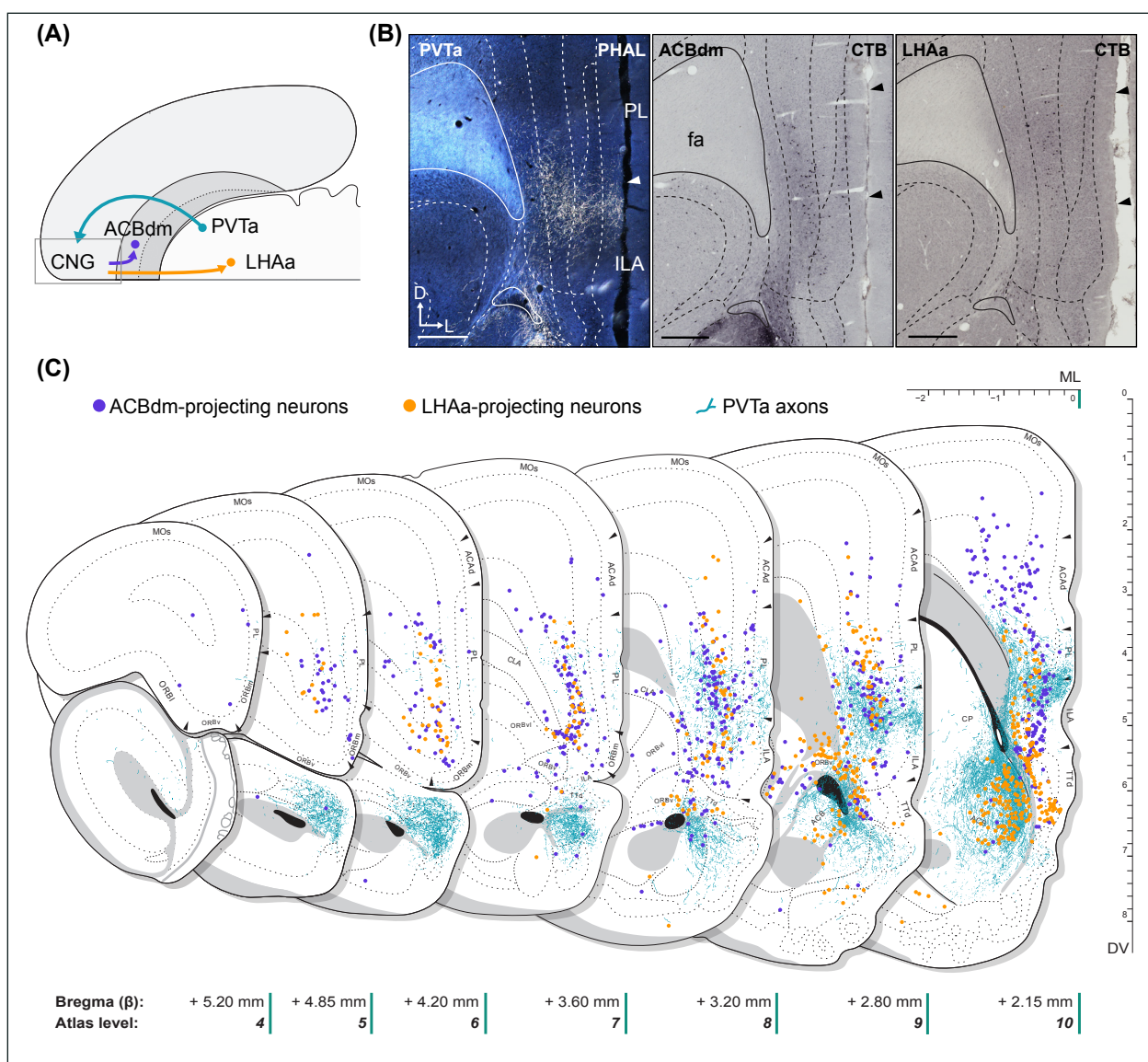


Figure 5. Convergent ACBdm, LHAA, and PVTa connections in the cytoarchitecturally defined cingulate region (CNG) [more loosely identified as the medial prefrontal cortex]. **(A)** Diagrammatic representation of experiments. Circles show injected regions and arrows show the direction of the connections. **(B)** Photomicrographs showing immunodetected PHAL and CTB in CNG at approximately +3.0 mm from bregma. Injection site locations are indicated with abbreviations in the upper-left corners and tracers are indicated in the upper-left corners of each image. Arrowheads point to boundary locations between cortical areas. Boundaries were determined using adjacent Nissl-stained sections. **(C)** Mapped distributions of PVTa axons (green), ACBdm- (purple) and LHAA-projecting (orange) neurons in the CNG. Note the overlap of each label in a subgenual part of the CNG. See Abbreviations for nomenclature. Scale bar: 500 μ m (B).

are highly segregated and formed distinct longitudinal columns. Cortical projections, on the other hand, tend to be more diffuse. This property complicates the definition of cortical projections to the ACBdm circuit from a top-down direction. In keeping with a bottom-up strategy, we defined cortical ACBdm circuit nodes as spaces that satisfied the following criteria: (i) Anterograde labeling from the PVTa, and (ii) retrograde labeling from both ACBdm and LHAA. We applied these criteria throughout the entire cortex and here we focus on three prominent zones of intersection.

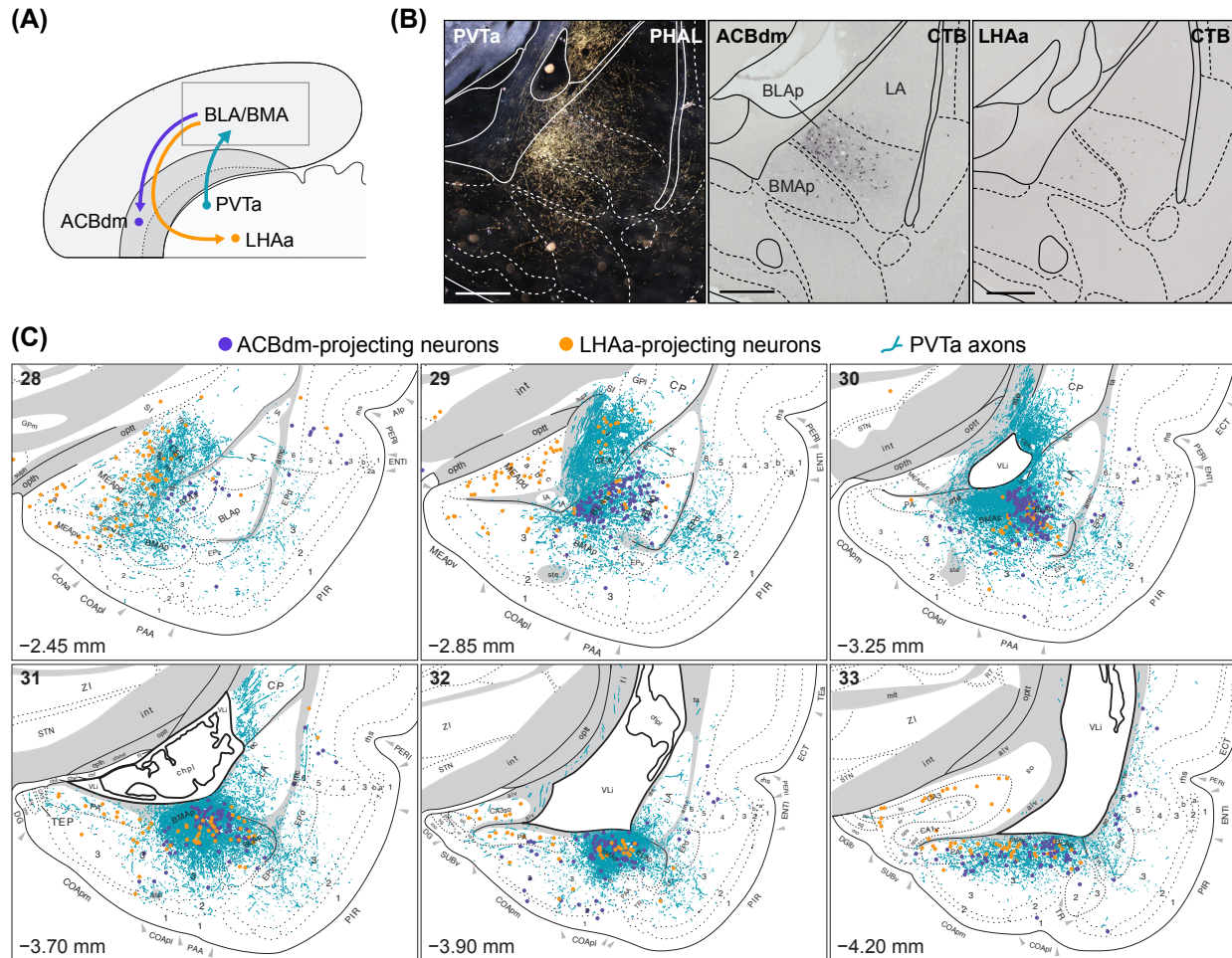


Figure 6. Convergent ACBdm, LHAa, and PVTa connections in amygdala. **(A)** Diagrammatic representation of experiments. Circles show injected regions and arrows show the direction of the connections. **(B)** Photomicrographs showing immunodetected PHAL and CTB in amygdala at approximately -3.5 mm from bregma. Injection site locations are indicated with abbreviations in the upper-left corners and tracers are indicated in the upper-left corners of each image. Boundaries were determined using adjacent Nissl-stained sections. **(C)** Mapped distributions of PVTa axons (green), ACBdm- (purple) and LHAa-projecting (orange) neurons in amygdala. Note the overlap of each label in a medial space between BLAp and BMAp. Values in lower-left corners indicate the approximate distance from bregma and corresponding atlas levels from Swanson (2018) are indicated in the upper-left corners of each panel. See Abbreviations for nomenclature. Scale bars: $500 \mu\text{m}$ (B).

We first examined the cingulate region (CNG) [informally, medial prefrontal cortex] for the ACBdm circuit criteria (**Fig. 5A**). Each criterion was satisfied for the deep layers of ventral CNG (**Fig. 5B**). CTB labeling from the ACBdm and LHAa was found throughout the CNG, including its anterior cingulate (ACA), prelimbic (PL), and infralimbic (ILA) divisions (**Fig. 5C**). Retrograde labeling from ACBdm and LHAa was mainly detected within layer 5 the anteroposterior extent of the ventral CNG. In contrast, PHAL-labeled PVTa axons were limited to a narrow space in the caudal half of CNG at $L8-10 AP \beta+2.15$ to $+3.20$. Nissl-based analysis showed the PVTa terminals are concentrated in each layer of a space along the boundary between the PL and ILA (**Fig. 5C**). The PVTa terminal field is bounded by the ‘dorsal peduncular cortex’ ventrally and is mostly contained within the ventral PL dorsally. Alternatively, the connectional overlap zone can be interpreted as a

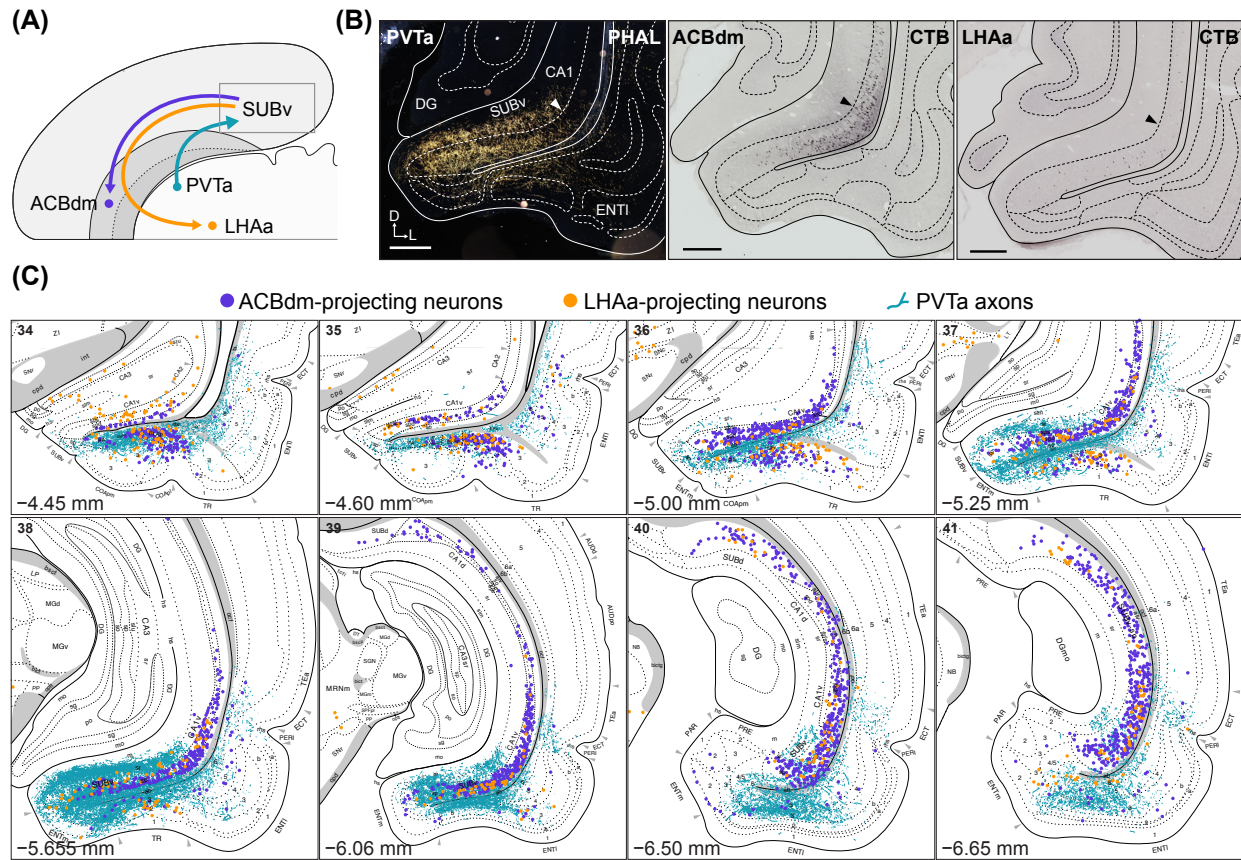


Figure 7. Convergent ACBdm, LHAa, and PVTa connections in hippocampus. **(A)** Diagrammatic representation of experiments. Circles show injected regions and arrows show the direction of the connections. **(B)** Photomicrographs showing immunodetected PHAL and CTB in SUBv at approximately -6.0 mm from bregma. Injection site locations are indicated with abbreviations in the upper-left corners and tracers are indicated in the upper-left corners of each image. Note the overlap of each label in a lateral aspect of the anterior SUBv. **(C)** Mapped distributions of PVTa axons (green), ACBdm- (purple) and LHAa- (orange) projecting neurons in hippocampus. Values in lower-left corners indicate the approximate distance from bregma and corresponding atlas levels from Swanson (2018) are indicated in the upper-left corners of each panel. See Abbreviations for nomenclature. Scale bars: 500 μm **(B)**.

‘subgenual’ part of the CNG.

Next, we examined the amygdalar complex for the ACBdm circuit inclusion criteria (**Fig. 6A**). Inclusion criteria were satisfied only in amygdalar regions posterior to the inferior horn of the lateral ventricle (**Fig. 6B**). PHAL labeling from PVTa and CTB labeling from ACBdm and LHAa were concentrated in a medial aspect of the basolateral amygdalar nucleus posterior part (BLAp). This labeling occurs predominantly at $L_{30-32}AP\beta_{-4.2}$ to -3.0 in a space that lies between BLAp and the basomedial nucleus posterior part (BMap) (**Fig. 6C**). We did not observe labeled connections with PVTa, LHAa, or ACBdm in more anterior parts of BLA, and these sub-regions were not included in our analysis. PHAL-labeled PVTa axons strongly label the central amygdalar nucleus (CEA), but this terminal field only contains some retrograde labeling from the LHAa. CTB labeling from LHAa is also prominent in the medial amygdalar nucleus (MEA) but this region only receives weak PVTa projections, and we detected no CTB labeling from ACBdm.

Finally, we examined for ACBdm circuit inclusion criteria in the hippocampal formation

(**Fig. 7A**). Injections into LHAA and ACBdm labeled both Ammon's horn field CA1 and ventral subiculum (SUBv) of hippocampus, but PHAL-labeled PVTa axons were only present in SUBv (**Fig. 7B**). Specifically, labeling from the three regions appeared concentrated in a lateral half of SUBv. Examined with higher spatial precision, the connectional overlap is restricted to the anterior pole of SUBv at $L^{37-40}AP^{\beta-6.06 \text{ to } -5.25}$ (**Fig. 7C**). CTB labeling from ACBdm and LHAA and notable PHAL label from PVTa also overlapped in the postpiriform transition area (TR; alternatively, the amygdalopiriform transition area) and deep layers of cortical amygdalar area $L^{34-38}AP^{\beta-5.65 \text{ to } -4.45}$. Prominent CTB labeling from ACBdm was present throughout the CA1 and posterior SUBv, but PVTa axons were undetected in these regions. Similarly, we detected dense PVTa axonal labeling in the entorhinal cortex, but these areas contained sparse CTB labeling from LHAA and ACBdm.

4: Discussion

In this study, we showed, using a bottom-up pathway tracing strategy, that a connectionally unique subdivision of ACB could be identified based on unidirectional connections with the SIm, LHAA, and PVTa. We also showed that SIm, LHAA, and PVTa connections in ACBdm form a longitudinal column along its entire anterior-posterior span. We then showed that the ACBdm-to-SIm pathway strongly overlaps in space with LHAA-projecting SI neurons. Finally, we identified topographically distinct cortical zones in ILA/PL, BMAp/BLAp, and SUBv that strongly connect with the ACBdm, LHAA, and PVTa regions of the ACBdm circuit. Taken together, the identified regions can be treated as nodes of a basal ganglia circuit. As such, the circuit can be divided into two major branches. A triple descending projection that is composed of a cortical ‘hyperdirect’ pathway, a striatal ‘direct pathway’ from ACBdm, and a pallidal ‘indirect pathway’ relayed through SIm (**Fig. 8a**). Each of the regions send projections to LHAA. The second branch is a thalamic feedback system. The PVTa, previously shown to receive inputs from SIm and LHAA, sends strong projections to each of the cortical and striatal parts of the ACBdm circuit (**Fig. 8b**). We use the term ‘circuit’ to refer to the closed-loop architecture connecting these regions. We discuss the implications of the triple descending circuit and the thalamic feedback loop in relation to affective and motivational processes.

4.1: Anatomical properties of the triple descending projection

We found that the ACBdm and SIm pathways to LHAA are characterized by high-density connections that are restricted to topographically distinct sub-domains. In their original description of basal ganglia circuits, Alexander, DeLong, and Strick (1986) emphasized functional segregation and parallel processing as central features of these circuits along with inhibitory ‘direct’ and disinhibitory ‘indirect’ pathways (Alexander & Crutcher, 1990). ACBdm projections arise from the well-studied medium-spiny neurons (MSN) that are capable of releasing GABA and neuropeptides (Castro & Bruchas, 2019). SI projection neurons are mostly GABAergic and typically exhibit high tonic activity (Mogenson et al., 1983). Moreover, another study found that ACB and SI projections

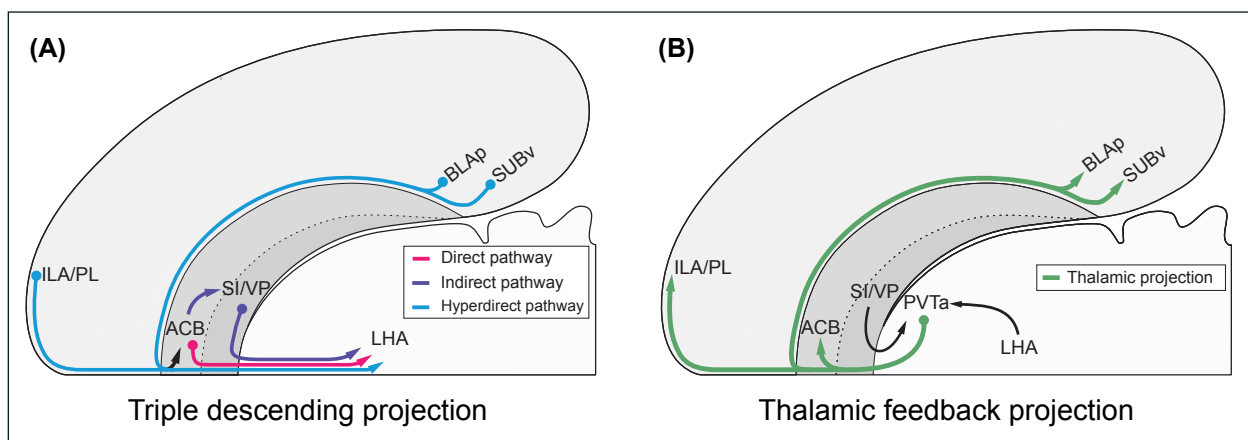


Figure 8. Schematic summary of findings. **(A)** A cortico-striatal-pallidal triple descending projecting converging on LHA. ACBdm and SIm respectively form inhibitory ‘direct’ and disinhibitory ‘indirect’ pathways to LHA. ILA/PL, BLAp/BMAp, and SUBv contribute ‘hyperdirect’ pathway projections to LHA. **(B)** SIm and LHA form feedback projections to PVTa which, in turn, sends strong projections to the corticostriatal parts of the ACBdm circuit. The triple descending projection and thalamic feedback projection form a closed-loop architecture that is defined along topographically distinct forebrain spaces.

to LHAA frequently converged on individual neurons (Prasad et al., 2020). The cortical outputs to ACBdm and the ‘hyperdirect’ pathway to LHAA are glutamatergic (Gerfen & Wilson, 1996) although there is one study showing the existence of GABAergic projections from ILA to ACBdm (Lee et al., 2014). Thus, our proposed triple descending projection aligns with the canonical features of the basal ganglia circuit and offers a potential connectional basis for the functional segregation phenomenon. The ACBdm-centered circuit described here is qualitatively similar to their ‘anterior cingulate circuit’ of primates (Alexander et al., 1986), whose functional role remains unclear.

Our connectional criteria identified a small subdomain positioned in a subgenual part of CNG (medial prefrontal cortex) between the PL and ILA at $L8-10AP^{\beta+2.15\text{ to }+3.20}$, we found another subdomain in amygdala between the BLA_p and BMA_p at $L8-10AP^{\beta-3.9\text{ to }-3.0}$. Topographic organization is well-recognized in CNG and BLA, but it is important to note that the cortical subdomains we identified also form segregated reciprocal connections with each other (Petrovich et al., 1996; Reppucci & Petrovich, 2016; Vertes, 2004). It is unclear how CNG–amygdalar reciprocal connections contribute to the ACBdm circuit. There is evidence that oscillation coupling between CNG and amygdala is associated with learning (Likhnik et al., 2014), and this may be relevant for top-down control of the ACBdm circuit. Anterior SUB_v at $L38-41AP^{\beta-6.7\text{ to }-5.6}$ is likewise bidirectionally connected with at least BMA_p (Canteras & Swanson, 1992; Petrovich et al., 1996), but it only forms unidirectional projections to PL and ILA (Hoover & Vertes, 2007; Jay & Witter, 1991; Vertes, 2004). Although CNG does not project to SUB_v, others have proposed that CNG could act on hippocampus through intermediate projections to the thalamic nucleus reuniens (McKenna & Vertes, 2004; Varela et al., 2014; Vertes et al., 2015). Taken together, the cortical subdomains of the ACBdm exhibit reciprocal connectivity that precisely aligns with the topographic sub-domains described here.

The ACBdm circuit sends a triple descending projection that converges on LHAA, ACBdm and SI projections to LHA are well-documented in rats and mice (Groenewegen et al., 1993; Hahn et al., 2022; Thompson & Swanson, 2010; Zahm & Heimer, 1993). Further, there is electrophysiological evidence showing that outputs from ACBdm and SI neurons frequently converge on individual LHA neurons (Prasad et al., 2020), although this was only examined for LHA Gad1-positive neurons caudal to LHAA at $L27-30AP^{\beta-1.92\text{ to }-3.24}$. There is also evidence of cell type-specific coding of ACB projections. D1 dopamine receptor-expressing neurons were shown to project to LHAA and a mixed population of D1 and D2 receptor-expressing neurons project to the SI (Gibson et al., 2018; Kupchik et al., 2015; O’Connor et al., 2015). Recent work in mice further adds that D3 dopamine receptor-expressing neurons also contribute ACBdm projections to LHA and SIm, this population co-expresses D1 and D2 receptors but mainly overlaps with the D1 population (Enriquez-Traba et al., 2025). Unlike striatum generally, neurochemical coding of the ACBdm does not provide a straightforward dichotomy between direct and indirect pathways and this has led some to conclude that other strategies are needed for ACB (Kupchik et al., 2015). As a related matter, it is still unclear whether ACBdm projections to SIm and LHAA arise from distinct populations. More work is needed to clarify the basic neurochemical and connectional properties of the ACBdm as a basal ganglia circuit. In this regard, it is important to note that all the present findings were made using conventional tracers. Thus, the ACBdm circuit reflects the global connectivity of the ACBdm, and highly specific parsing was achieved without using cell type-specific methods.

At present, there does not appear to be an unambiguous neurochemical marker for ACBdm. An emerging literature based on single-cell transcriptomic analysis of striatum consistently detects

a unique cluster of MSNs centered in the ACBdm of rodents and primates. These are referred to as hybrid or ‘eccentric’ MSNs based on co-expression of D1 and D2 receptors and their tendency to form distant clusters from the canonical D1- and D2-enriched populations (Gokce et al., 2016; He et al., 2021; Saunders et al., 2018; Stanley et al., 2020). In mouse ACB, the D1/D2 hybrid population is concentrated in the ACBdm (Gagnon et al., 2017). Transcriptomic analysis of striatal interneurons similarly isolates a cluster of *Tac3* neurons in humans (Garma et al., 2024), which appears to be evolutionarily conserved among mammals (Corrigan et al., 2024) and expressed in the ACBdm of primates (He et al., 2021). Prominent genes from the D1/D2 hybrid clusters are strongly expressed throughout the anterior-posterior extent of ACBdm as shown here with connections, offering potential neurochemical markers for the ACBdm column. See, for example, the distribution patterns of *Stard5* or *Tac2* (a rodent ortholog of the primate *Tac3*). Importantly, the findings from this literature support our overall conclusions regarding the spatial description of the ACBdm as a longitudinal column and they highlight a unique profile for gene-expression in addition to connectivity.

4.2: Anatomical properties of the thalamic feedback loop

We showed, using a well-contained PHAL injection into PVTa, that its projections to cortex, amygdala, and hippocampal formation are largely restricted to the cortical components of the ACBdm circuit. PHAL-labeled PVTa axons in striatum densely terminated in a longitudinal span we designate as the ACBdm column. Our description of PVTa projections agrees with previous investigations of PVT outputs, revealed using both anterograde and retrograde tracing (Li & Kirouac, 2008; Vertes & Hoover, 2008). Among the cortical areas we mentioned, PVTa is reciprocally connected with PL, ILA, SUBv, but not BMAp or BLAp (Canteras & Swanson, 1992; Petrovich et al., 1996; Vertes, 2004). We observed no PVTa projections to the SI or LHAA (Vertes & Hoover, 2008). Thus, PVTa projections appear to mainly influence cortical and striatal components of the ACBdm circuit.

Given the centrality of PVTa projections in the ACBdm circuit, it is important to consider the potential contribution of axon collaterals. A dual retrograde tracing study showed only small overlap in PVTa neurons projecting to CNG and ACBdm (Bubser & Deutch, 1998). Dual retrograde tracing studies generally found partial overlap between ACBdm-projecting PVT neurons and retrograde labeling from the central amygdalar nucleus and bed nuclei of the stria terminalis (Dong et al., 2017; Freedman & Cassell, 1994). It remains to be determined whether PVTa neurons form collaterals in connection with BMAp, BLAp, and SUBv in addition to CNG and ACBdm. At present, PVTa appears more likely to exert discrete control over individual ACBdm circuit nodes rather than simultaneous influencing the circuit.

Previous work has shown that SI and LHAA also project to the PVTa (Li & Kirouac, 2012; Thompson & Swanson, 2010). However, the PVTa receives broad inputs from hypothalamus beyond LHAA (Li et al., 2014). PVTa inputs arrive from the hypocretin/orexin and melanin-concentrating hormone populations, tyrosine hydroxylase neurons of zona incerta (Bono et al., 2024), suprachiasmatic nucleus (Canteras et al., 2011), Agouti-related peptide and pro-opiomelanocortin neurons of the arcuate nucleus (Freedman & Cassell, 1994). The PVTa is understood as an integration site for a wide range of bottom-up inputs that convey diverse information regarding the animal’s internal state (Kelley et al., 2005). PVTa can thus integrate internal state information to exert specific influence via top-down control of corticostriatal connections, in effect shaping local dynamics and competition between ACBdm and other basal ganglia circuits (McNally, 2021;

Millan et al., 2017).

4.3: Functional properties of the ACBdm triple descending projection

Each component of the ACBdm circuit plays a role in affective and motivational processes, but they are often studied separately and there is no clear unifying framework for these functions. In our treatment of the ACBdm triple descending projection and thalamic feedback loop, it is critical to treat stereotaxic space as a shared reference between multimodal datasets (Khan, 2013). We described ACBdm circuit nodes with topographic precision that can relate to sites described in brain manipulation and recording experiments. We therefore prioritize studies in which stereotaxic information (i.e. empirically determined cannula placements) was well-documented.

It has been long established that ACBdm plays a role in feeding behaviors (Kelley et al., 2005; Maldonado-Irizarry et al., 1995), and ACBdm control of feeding is mediated by its connections with LHAA (Stratford & Kelley, 1999). The CNG has also been shown to participate in non-homeostatic feeding induced by local injections of mu-opioid receptor (MOR) agonists (Castro & Berridge, 2017; Mena et al., 2011; Mena et al., 2013). Opioid-elicited feeding was especially effective when injections targeted the PL and ILA (Mena et al., 2011), and is blocked by simultaneously inactivating the LHA whereas inactivating the anterior part of ACBdm has no effect (Mena et al., 2013). In contrast, feeding elicited by MOR agonism in ACB is blocked by simultaneously inactivating the BLA (Parker et al., 2015). PL and ILA also play a role in non-homeostatic feeding that results from cued potentiation. Both regions show strong Fos activation upon presentation of food-paired cues (Cole et al., 2015), and contextually-conditioned feeding is disrupted by neurotoxic lesions to the medial prefrontal cortex (Petrovich et al., 2007). Similarly, an anatomical disconnection study has shown the necessity of BLA connections with LHA for cue-potentiated feeding (Petrovich et al., 2002).

An overlapping literature examines the effect of MOR stimulation on affective responses. Studies conducted by the Berridge lab systematically described the effects of injecting the MOR agonist, DAMGO, on taste reactivity and avoidance behaviors (Morales & Berridge, 2020). Of note, this work uncovered hedonic ‘hotspots’, or circumscribed zones that enhance the hedonic impact of food. Specifically, hedonic hotspots were identified in CNG (Castro & Berridge, 2017), ACBdm (Peciña & Berridge, 2005), and SI (Smith & Berridge, 2005). Alignment of hotspot stereotaxic information with the present ACBdm circuit leads to several observations. First, our connection-defined ACBdm column can be divided across an anterior ‘hotspot’ and a posterior ‘coldspot’ that elicits aversive taste responses. In addition to acting as a hedonic coldspot, inhibition of the posterior ACBdm induces anti-predator defensive behaviors (Reynolds & Berridge, 2001, 2002). Next, we showed that the anterior division of ACBdm projects to the SIm, which is a ventral pallidal ‘coldspot’ for both feeding and taste reactivity after MOR stimulation (Smith & Berridge, 2005). The anterior ACBdm is the primary source of GABA in the medial SIm. Thus, ACBdm can potentially control feeding by inhibiting the anterior SIm coldspot. Accordingly, GABA antagonism in the SIm increases feeding (Smith & Berridge, 2005). It is therefore possible that ACBdm exert bidirectional control over feeding and hedonic responses through ‘go’ and ‘no-go’ pathways through LHAA and SIm, respectively. To this point, electrical stimulation of ACBdm was shown to produce mixed effects on downstream LHA neurons (Mogenson et al., 1983). Finally, the ACBdm circuit model would further predict that SUBv, BMAp/BLAp, and LHAA could play roles in affective processes.

4.4: Functional properties of ACBdm as a basal ganglia closed-loop circuit

Recent investigations of basal ganglia circuits have clarified two fundamental features of basal ganglia circuits. Studies of CP have shown that striatopallidal projections form closed-loop architectures with downstream midbrain and thalamic regions, and different parts of CP form parallel loops that remain segregated at every level of the basal ganglia circuit (Foster et al., 2021; Lee et al., 2020). Moreover, anatomically segregated basal ganglia circuits also control distinct functional and behavioral outputs (Lee et al., 2020), in agreement with the formulation of Alexander, DeLong, and Strick (1986). We showed that topographically organized and segregated connections, as well as the triple descending projection motif, can be applied to the ACBdm. The implications of such anatomical and functional segregation between basal ganglia circuits are unclear. It is also unclear whether computational features of basal ganglia closed-loop circuits can generalize to the ACBdm circuit. Additionally, there are many aspects of basal ganglia cell type and synaptic organization, such as the inclusion of recently discovered arkypallidal neurons, that have not been addressed here (Fang & Creed, 2024; Guilhemsang & Mallet, 2024). Nevertheless, one major implication of our work is that manipulations to individual components of the ACBdm circuit can have effects on the entire circuit based on the closed-loop architecture. For example, unilateral infusions of muscimol into ACBdm leads to marked Fos increases in LHA, PVTa, lateral habenula (LH) (Stratford, 2005).

The ACBdm circuit architecture features multiple dense glutamatergic projections from PVTa, SUBv, ILA/PL, and BLAp/BMAp converging on the ACBdm. As mentioned above, there is a high degree of reciprocal connectivity among the corticothalamic regions but the significance of this remains unclear. One possibility is that reciprocal connectivity can facilitate synchronous and convergent excitatory inputs to ACBdm MSNs that are required to transition into depolarized ‘up-states’ (Fang & Creed, 2024). This possibility is supported by observations that individual ACBdm MSNs receive converging synaptic inputs from CNG, SUBv, and BLAp (French et al., 2003; French & Totterdell, 2002).

4.5: Methodological considerations

We uncovered a ACBdm circuit using a Nissl-based method to localize tracers. We were primarily interested in the spatial organization of traced axons and retrograde labeling; we did no further work to confirm synaptic formation. We interpreted the presence of axon terminals (i.e., extensive branching and varicosities) to indicate relevant spaces in which putative synaptic contacts are likely to be found. Previous work has suggested that varicosities detected with light microscopy are highly correlated with synaptic contacts when examined under electron microscopy (Wouterlood & Groenewegen, 1985). Synaptic connections were previously demonstrated using electron microscopy and patch-clamp physiology for each of the pathways we described. Nevertheless, additional work is needed for the goal of establishing the microcircuit and synaptic properties of the ACBdm circuit. ACBdm connections can also be studied using trans-synaptic anterograde tracing where connections are strictly unidirectional (Zingg et al., 2017; 2020) and monosynaptic retrograde tracing (Wickersham et al., 2007).

We defined the ACBdm circuit based on connections with ACBdm, LHAA, and PVTa. This allowed us to identify topographically distinct cortical areas of the ACBdm circuit that can exhibit closed-loop architecture. Similar criteria can be used to identify adjacent basal ganglia loops. We noted, for example, strong PVTa projections to the CEA. CEA is not connected with ACBdm

but was densely labeled with CTB from the LHAA, particularly in its lateral part. Our bottom-up strategy can be applied to establish additional basal ganglia circuits. It is important to note that some regions, like much of CNG and CA1, contained retrograde labeling from ACBdm and LHAA but lacked anterograde labeling from PVTa. We can surmise that these regions are unlikely to show properties of closed-loop architectures for the nodes we examined, but they are nevertheless strongly connected with the ACBdm circuit and further work can elaborate the role regions outside the PVTa feedback loop.

Our description of the ACBdm circuit was limited to forebrain structures. There are well-known downstream projections, such as to the ventral tegmental area (VTA), LH, and periaqueductal grey. Among these, omission of VTA, which projects to most of the ACBdm circuit (Swanson, 1982), may seem objectionable and requires some explanation. Previous work on the ACBdm circuit showed that ACBdm projections to VTA were sparse and a large retrograde injection centered in VTA extensively labeled ACB except for ACBdm (Thompson & Swanson, 2010). A similar observation can be made in the ACBdm of mice after retrobead injections into VTA, although this was not a conclusion from the study (Enriquez-Traba et al., 2024). We similarly observed sparse projections to VTA in our anterograde tracer injections into ACBdm, SIm, mPFC. Instead, these regions send dense projections to LHA. Finally, the VTA reportedly lacks projections to the PVT (Li et al., 2014), which is arguably the only route for thalamic feedback into the ACBdm circuit. The VTA nevertheless receives a major projection from the LHAA and can be considered a feedback system of its own.

4.6: Concluding remarks

We identified a closed-loop circuit that is reminiscent of the ‘limbic’ circuit from early descriptions of basal ganglia circuits (Alexander & Crutcher, 1990; Alexander et al., 1986). If basal ganglia motifs are evolutionally conserved, it is possible that further elucidation of basal ganglia circuits can be a basis for clarifying brain region homologies across mammals (Swanson & Hof, 2019; Tang et al., 2024). A better understanding of the ACBdm circuit could also lead to insights into disordered states. The ACBdm circuit has considerable overlap with the circuits implicated in relapse to drug seeking after extinction (Marchant et al., 2019), and is a potential neural substrate for the effective amelioration of treatment-resistant depression (Riva-Posse et al., 2020).

Acknowledgments

This work was supported by funds awarded to AMK from the U. S. National Institutes of Health (NIH) (SC1GM127251; R01MH114961) and the Howard Hughes Medical Institute (HHMI) for the UTEP PERSIST Brain Mapping & Connectomics Laboratory (see below). KN was supported by NIH SC1GM127251, the Department of Biological Sciences, and the Eloise E. and Patrick Wieland Fellowship at UTEP, and is currently supported by the Scientific Director's Fellowship for Diversity in Research and the Center on Compulsive Behaviors at the NIH. Work performed in the BMC Laboratory was conducted within UTEP PERSIST (Program to Educate and Retain Students in STEM Tracks), a training program funded by HHMI grant 52008125 (PI: S. B. Aley, Co-PIs: L. Echegoyen, A. M. Khan, D. Villagrán, E. Greenbaum). KN and VIN served as PERSIST Teaching Assistants and LSA, JMGR, DS, and ART are PERSIST Alumni. VIN has also been supported by a Doctoral Excellence Fellowship and VIN, ART, and DS are fellows of the UTEP RISE (Research Initiative for Scientific Enhancement) program, which is funded by the National Institute of General Medical Sciences of the NIH (R25GM069621; PI: R. Aguilera). LSA was supported by a PRELS Fellowship (Post-baccalaureate Research opportunities for LSAMP students; #EES-2204750) under the University of Texas System Louis Stokes Alliances for Minority Participation Program (UT System LSAMP) program funded by the National Science Foundation (HRD-1826745; PI; B. C. Flores). This work was also supported by the Border Biomedical Research Center, which is funded by the National Institute on Minority Health and Health Disparities of the NIH (2U54MD007592; PI: R. A. Kirken). Pending confirmatory work for this project is also being supported by the Intramural Research Program of the NIDA-NIH (Yavin Shaham). We thank Yavin Shaham, Alexander Friedman, and Huiling Wang for helpful comments on the manuscript, and Richard H. Thompson and Larry W. Swanson for conversations concerning their proposed forebrain circuit model. All BM4 atlas maps were modified and/or reproduced with permission under the conditions outlined by a Creative Commons BY-NC 4.0 license (<https://creativecommons.org/licenses/by-nc/4.0/>).

Abbreviations

AAA	<i>anterior amygdalar area (Gurdjian, 1928)</i>
ACA	<i>anterior cingulate area (Brodmann, 1909)</i>
ACAd	<i>anterior cingulate area dorsal part (Krettek & Price, 1977)</i>
ACB	<i>accumbens nucleus (Ziehen, 1897-1901)</i>
aco	<i>olfactory limb of anterior commissure (>1840)</i>
AD	<i>anterodorsal thalamic nucleus (>1840)</i>
AHN	<i>anterior hypothalamic nucleus (>1840)</i>
AHNa	<i>anterior hypothalamic nucleus anterior part (>1840)</i>
AHNc	<i>anterior hypothalamic nucleus central part (>1840)</i>
AHNp	<i>anterior hypothalamic nucleus posterior part (>1840)</i>
Alp	<i>posterior agranular insular area (Krettek & Price, 1977)</i>
alv	<i>alveus (Burdach, 1822)</i>
AM	<i>anteromedial thalamic nucleus (>1840)</i>
amc	<i>amygdalar capsule (Swanson, 1998)</i>
AUDd	<i>dorsal auditory areas (Sally & Kelly, 1988)</i>
AUDpo	<i>posterior auditory area (Doron et al., 2002)</i>
AV	<i>anteroventral thalamic nucleus (>1840)</i>
BLAa	<i>basolateral amygdalar nucleus anterior part (>1840)</i>
BLAp	<i>basolateral amygdalar nucleus posterior part (>1840)</i>
BM4	Brain Maps 4.0
BMAa	<i>basomedial amygdalar nucleus anterior part (>1840)</i>
BMAp	<i>basomedial amygdalar nucleus posterior part (>1840)</i>
BST	<i>bed nuclei of terminal stria (Gurdjian, 1925)</i>
CA1	<i>Ammon's horn field CA1 (Lorente de Nó, 1934)</i>
CA1d	<i>Ammon's horn field CA1 dorsal part (Risold & Swanson, 1996)</i>
CA1v	<i>Ammon's horn field CA1 ventral part (Risold & Swanson, 1996)</i>
CA2	<i>Ammon's horn field CA2 (Lorente de Nó, 1934)</i>
CA3so	<i>Ammon's horn field CA3 stratum oriens (>1840)</i>
CEA	<i>central amygdalar nucleus (Johnston, 1923)</i>
CEAc	<i>central amygdalar nucleus capsular part (McDonald, 1982)</i>
CEAl	<i>central amygdalar nucleus lateral part (Swanson, 1992)</i>
CEAm	<i>central amygdalar nucleus medial part (McDonald, 1982)</i>
CLA	<i>claustrum (Burdach, 1822)</i>
CM	<i>central medial thalamic nucleus (Rioch, 1929)</i>
COAa	<i>cortical amygdalar area anterior part (>1840)</i>
COApl	<i>cortical amygdalar area posterior part lateral zone (>1840)</i>
COApm	<i>cortical amygdalar area posterior part medial zone (>1840)</i>
CP	<i>caudoputamen (Heimer & Wilson, 1975)</i>
cpd	<i>cerebral peduncle (Tarin, 1753)</i>
CTB	cholera toxin B subunit
DG	<i>dentate gyrus (>1840)</i>
DGmo	<i>dentate gyrus molecular layer (>1840)</i>
DGsg	<i>dentate gyrus granule cell layer (>1840)</i>
ACBdm	<i>accumbens nucleus (Ziehen, 1897–1901), dorsomedial column</i>

Abbreviations (continued)

ec	<i>external capsule (Burdach, 1822)</i>
ECT	<i>ectorhinal area (Brodmann, 1909)</i>
ENTl	<i>entorhinal area lateral part (>1840)</i>
ENTm	<i>entorhinal area medial part (>1840)</i>
EPd	<i>endopiriform nucleus dorsal part (Krettek & Price, 1978)</i>
EPv	<i>endopiriform nucleus ventral part (Krettek & Price, 1978)</i>
frf	<i>radiation of corpus callosum frontal forceps (>1840)</i>
GPl	<i>lateral globus pallidus (>1840)</i>
GPm	<i>medial globus pallidus (>1840)</i>
I	<i>internuclear hypothalamic area (Swanson, 2004)</i>
IA	<i>intercalated amygdalar nuclei (>1840)</i>
IAD	<i>interanterodorsal thalamic nucleus (>1840)</i>
ILA	<i>infralimbic area (Rose & Woolsey, 1948)</i>
int	<i>internal capsule (Burdach, 1822)</i>
isl	<i>islands of Calleja (>1840)</i>
LA	<i>lateral amygdalar nucleus (>1840)</i>
LHA	<i>lateral hypothalamic area (Nissl, 1913)</i>
LHAa	<i>lateral hypothalamic area anterior group anterior region (Swanson, 2004)</i>
LHAai	<i>lateral hypothalamic area anterior group anterior region intermediate zone (Swanson, 2004)</i>
LHAav	<i>lateral hypothalamic area anterior group anterior region ventral zone (Swanson, 2004)</i>
LHAjp	<i>lateral hypothalamic area middle group medial tier juxtaparaventricular region (Swanson, 2004)</i>
LP	<i>lateral posterior thalamic nucleus (>1840)</i>
MD	<i>mediodorsal thalamic nucleus (>1840)</i>
MDm	<i>mediodorsal thalamic nucleus medial part (>1840)</i>
MEA	<i>medial amygdalar nucleus (Johnston, 1923)</i>
MEAd	<i>medial amygdalar nucleus anterodorsal part (>1840)</i>
MEApd	<i>medial amygdalar nucleus posterodorsal part (>1840)</i>
MEApd.a	<i>medial amygdalar nucleus posterodorsal part sublayer a (>1840)</i>
MEApd.b	<i>medial amygdalar nucleus posterodorsal part sublayer b (>1840)</i>
MEApd.c	<i>medial amygdalar nucleus posterodorsal part sublayer c (>1840)</i>
MEApv	<i>medial amygdalar nucleus posteroventral part (>1840)</i>
MGd	<i>medial geniculate complex dorsal part (>1840)</i>
MGv	<i>medial geniculate complex ventral part (>1840)</i>
MOR	<i>mu-opioid receptor</i>
MOs	<i>secondary somatomotor areas (>1840)</i>
MRNm	<i>midbrain reticular nucleus (>1840)</i>
NB	<i>nucleus of brachium of inferior colliculus (>1840)</i>
NC	<i>nucleus circularis (>1840)</i>
NDB	<i>diagonal band nucleus (>1840)</i>
oph	<i>hypothalamic optic tract (Swanson, 2015)</i>
optt	<i>thalamic optic tract (Swanson, 2015)</i>

Abbreviations (continued)

ORBl	<i>lateral orbital area (Krettek & Price, 1977)</i>
ORBm	<i>medial orbital area (Krettek & Price, 1977)</i>
ORBv	<i>ventral orbital area (Krettek & Price, 1977)</i>
ORBvl	<i>ventrolateral orbital area (Krettek & Price, 1977)</i>
OT	<i>olfactory tubercle (Calleja, 1893)</i>
PA	<i>posterior amygdalar nucleus (Canteras et al., 1992)</i>
PAA	<i>piriform-amygdalar area (Canteras et al., 1992)</i>
PAR	<i>parasubiculum (>1840)</i>
PERI	<i>perirhinal area (Brodmann, 1909)</i>
PHAL	<i>Phaseolus vulgaris leucoagglutinin</i>
PIR	<i>piriform area (Smith, 1919)</i>
PL	<i>prelimbic area (Brodmann, 1909)</i>
pofh	<i>hypothalamic postcommissural fornix (Swanson, 2015)</i>
PP	<i>peripeduncular nucleus (>1840)</i>
PRE	<i>presubiculum (Swanson & Cowan, 1977)</i>
PS	<i>parastrial nucleus (Simerly et al., 1984)</i>
PT	<i>paratenial nucleus (>1840)</i>
PVa	<i>periventricular hypothalamic nucleus anterior part (Swanson, 2018)</i>
PVH	<i>paraventricular hypothalamic nucleus (>1840)</i>
PVHdp	<i>paraventricular hypothalamic nucleus descending division dorsal parvicellular part (>1840)</i>
PVHmpd	<i>paraventricular hypothalamic nucleus parvicellular division medial parvicellular part dorsal zone (Simmons & Swanson, 2008)</i>
PVHpm	<i>paraventricular hypothalamic nucleus magnocellular division posterior magnocellular part medial zone (>1840)</i>
PVHpv	<i>paraventricular hypothalamic nucleus parvicellular division periventricular part (>1840)</i>
PVTa	<i>paraventricular thalamic nucleus (>1840) anterior part</i>
RCH	<i>lateral hypothalamic area anterior group retrochiasmatic area (>1840)</i>
rhs	<i>rhinal sulcus (>1840)</i>
RT	<i>reticular thalamic nucleus (>1840)</i>
SBPV	<i>subparaventricular zone (Watts et al., 1987)</i>
SF	<i>septofimbrial nucleus (>1840)</i>
SGN	<i>suprageniculate nucleus (>1840)</i>
SI	<i>substantia innominata or innominate substance (Schwalbe, 1881)</i>
SIm	<i>substantia innominata medial part</i>
smh	<i>hypothalamic medullary stria (Swanson, 2018)</i>
SNC	<i>substantia nigra compact part (Sano, 1910)</i>
SNr	<i>substantia nigra reticular part (Sano, 1910)</i>
SOp	<i>supraoptic nucleus principal part (Swanson, 2018)</i>
SPFpl	<i>subparafascicular nucleus parvicellular part lateral division (>1840)</i>
ste	<i>endbrain terminal stria (Swanson, 2015)</i>
STN	<i>subthalamic nucleus (>1840)</i>
SUBd	<i>subiculum dorsal part (Swanson & Cowan, 1975)</i>

Abbreviations (continued)

SUBv	<i>subiculum ventral part (Swanson & Cowan, 1975)</i>
suph	<i>hypothalamic supraoptic decussations (Swanson, 2018)</i>
TEa	<i>temporal association areas (Swanson, 1992)</i>
TEP	<i>temporal pole (Broca, 1878)</i>
TR	<i>postpiriform transition area (Canteras et al., 1992)</i>
TTd	<i>tenia tecta dorsal part (Swanson, 1992)</i>
VL	<i>lateral ventricle (Vesalius, 1543)</i>
VLi	<i>inferior horn of lateral ventricle (Bell, 1802)</i>
vlt	<i>ventrolateral hypothalamic tract (Swanson, 2004)</i>
VP	ventral pallidum
VTA	<i>ventral tegmental area (Tsai, 1925)</i>
ZI	<i>zona incerta (>1840)</i>
β	bregma

References

Alexander, G. E., & Crutcher, M. D. (1990). Functional architecture of basal ganglia circuits: neural substrates of parallel processing. *Trends in Neuroscience*, 13(7), 266–271. [https://doi.org/10.1016/0166-2236\(90\)90107-1](https://doi.org/10.1016/0166-2236(90)90107-1)

Alexander, G. E., DeLong, M. R., & Strick, P. L. (1986). Parallel organization of functionally segregated circuits linking basal ganglia and cortex. *Annual Review of Neuroscience*, 9, 357–381. <https://doi.org/10.1146/annurev.ne.09.030186.002041>

Berendse, H. W., Galis-de Graaf, Y., & Groenewegen, H. J. (1992). Topographical organization and relationship with ventral striatal compartments of prefrontal corticostriatal projections in the rat. *The Journal of Comparative Neurology*, 316(3), 314–347. <https://doi.org/10.1002/cne.903160305>

Bono, B. S., Negishi, K., Dumiaty, Y., Ponce, M. S., Akinbode, T. C., Baker, K. S., *et al.*, (2024). Brain-wide projections of mouse dopaminergic zona incerta neurons. *bioRxiv*, 2024.2009.2006.611701. <https://doi.org/10.1101/2024.09.06.611701>

Broca, P. P. (1878) Nomenclature cérébrale: dénomination et subdivision des hémisphères et des anfractuosités de la surface. *Revue d'Anthropologie*, 1, 193–236.

Brodmann, K. (1909). *Vergleichende Lokalisationslehre der Grosshirnrinde in ihren Prinzipien Dargestellt auf Grund des Zellenbaues* (Barth, Leipzig).

Bubser, M., & Deutch, A. Y. (1998). Thalamic paraventricular nucleus neurons collateralize to innervate the prefrontal cortex and nucleus accumbens. *Brain Research*, 787(2), 304–310. [https://doi.org/10.1016/s0006-8993\(97\)01373-5](https://doi.org/10.1016/s0006-8993(97)01373-5)

Bell, C. (1802). *The Anatomy of the Brain, Explained in a Series of Engravings* (Longman & Rees, London). *Facsimile, Engravings of the Brain and Nerves*, published by The Classics of Medicine Library, Birmingham, 1982.

Burdach, K.F. (1822). *Vom Baue und Leben des Gehirns* (Dyk'schen Buchhandlung, Leipzig).

Calleja, C. (1893). *La Región Olfatoria del Cerebro* (Moya, Madrid).

Canteras, N. S., Simerly, R. B., & Swanson, L. W. (1992). The connections of the posterior nucleus of the amygdala. *The Journal of Comparative Neurology*, 324, 143–179. <https://doi.org/10.1002/cne.903240203>

Canteras, N. S., Ribeiro-Barbosa, E. R., Goto, M., Cipolla-Neto, J., & Swanson, L. W. (2011). The retinohypothalamic tract: comparison of axonal projection patterns from four major targets. *Brain Research Reviews*, 65(2), 150–183. <https://doi.org/10.1016/j.brainresrev.2010.09.006>

Canteras, N. S., & Swanson, L. W. (1992). Projections of the ventral subiculum to the amygdala, septum, and hypothalamus: a PHAL anterograde tract-tracing study in the rat. *The Journal of Comparative Neurology*, 324(2), 180–194. <https://doi.org/10.1002/cne.903240204>

Castro, D. C., & Berridge, K. C. (2017). Opioid and orexin hedonic hotspots in rat orbitofrontal cortex and insula. *Proceedings of the National Academy of Sciences, USA*, 114(43), E9125–E9134.

<https://doi.org/10.1073/pnas.1705753114>

Castro, D. C., & Bruchas, M. R. (2019). A motivational and neuropeptidergic hub: Anatomical and functional diversity within the nucleus accumbens shell. *Neuron*, *102*(3), 529–552. <https://doi.org/10.1016/j.neuron.2019.03.003>

Cole, S., Hobin, M. P., & Petrovich, G. D. (2015). Appetitive associative learning recruits a distinct network with cortical, striatal, and hypothalamic regions. *Neuroscience*, *286*, 187–202. <https://doi.org/10.1016/j.neuroscience.2014.11.026>

Corrigan, E. K., DeBerardine, M., Poddar, A., Turrero Garcia, M., Schmitz, M. T., Harwell, C. C., *et al.*, (2024). Conservation, alteration, and redistribution of mammalian striatal interneurons. *bioRxiv* 2024.07.29.605664. <https://doi.org/10.1101/2024.07.29.605664>

Dong, X., Li, S., & Kirouac, G. J. (2017). Collateralization of projections from the paraventricular nucleus of the thalamus to the nucleus accumbens, bed nucleus of the stria terminalis, and central nucleus of the amygdala. *Brain Structure and Function*, *222*(9), 3927–3943. <https://doi.org/10.1007/s00429-017-1445-8>

Doron, N. N., LeDoux, J. E., & Semple, M.N. (2002). Redefining the tonotopic core of rat auditory cortex: physiological evidence for a posterior field. *The Journal of Comparative Neurology*, *453*, 345–360. <https://doi.org/10.1002/cne.10412>

Enriquez-Traba, J., Arenivar, M., Yarur-Castillo, H. E., Noh, C., Flores, R. J., Weil, T., Roy, S., *et al.*, (2025). Dissociable control of motivation and reinforcement by distinct ventral striatal dopamine receptors. *Nature Neuroscience*, *28*, 105–121. <https://doi.org/10.1038/s41593-024-01819-9>

Fang, L. Z., & Creed, M. C. (2024). Updating the striatal-pallidal wiring diagram. *Nature Neuroscience*, *27*(1), 15–27. <https://doi.org/10.1038/s41593-023-01518-x>

Foster, N. N., Barry, J., Korobkova, L., Garcia, L., Gao, L., Becerra, M., *et al.*, (2021). The mouse cortico-basal ganglia-thalamic network. *Nature*, *598*(7879), 188–194. <https://doi.org/10.1038/s41586-021-03993-3>

Freedman, L. J., & Cassell, M. D. (1994). Relationship of thalamic basal forebrain projection neurons to the peptidergic innervation of the midline thalamus. *The Journal of Comparative Neurology*, *348*(3), 321–342. <https://doi.org/10.1002/cne.903480302>

French, S. J., Hailstone, J. C., & Totterdell, S. (2003). Basolateral amygdala efferents to the ventral subiculum preferentially innervate pyramidal cell dendritic spines. *Brain Research*, *981*(1–2), 160–167. [https://doi.org/10.1016/s0006-8993\(03\)03017-8](https://doi.org/10.1016/s0006-8993(03)03017-8)

French, S. J., & Totterdell, S. (2002). Hippocampal and prefrontal cortical inputs monosynaptically converge with individual projection neurons of the nucleus accumbens. *The Journal of Comparative Neurology*, *446*(2), 151–165. <https://doi.org/10.1002/cne.10191>

Gagnon, D., Petryszyn, S., Sanchez, M. G., Bories, C., Beaulieu, J. M., De Koninck, Y., *et al.*, (2017). Striatal neurons expressing D(1) and D(2) receptors are morphologically distinct and differently affected by dopamine denervation in mice. *Scientific Reports*, *7*, 41432. <https://doi.org/10.1038/s41598-017-04143-2>

[org/10.1038/srep41432](https://doi.org/10.1038/srep41432)

Garma, L. D., Harder, L., Barba-Reyes, J. M., Marco Salas, S., Diez-Salguero, M., Nilsson, M., *et al.*, (2024). Interneuron diversity in the human dorsal striatum. *Nature Communications*, 15(1), 6164. <https://doi.org/10.1038/s41467-024-50414-w>

Gerfen, C. R., & Sawchenko, P. E. (1984). An anterograde neuroanatomical tracing method that shows the detailed morphology of neurons, their axons and terminals: immunohistochemical localization of an axonally transported plant lectin, *Phaseolus vulgaris* leucoagglutinin (PHA-L). *Brain Research*, 290(2), 219–238. [https://doi.org/10.1016/0006-8993\(84\)90940-5](https://doi.org/10.1016/0006-8993(84)90940-5)

Gerfen, C. R., & Wilson, C. J. (1996). Chapter II. The basal ganglia. In: L. W. Swanson, A. Björklund, & T. Hökfelt (Eds.), *Handbook of Chemical Neuroanatomy (Vol. 12)*, pp. 371–468. Elsevier. [https://doi.org/10.1016/S0924-8196\(96\)80004-2](https://doi.org/10.1016/S0924-8196(96)80004-2)

Gibson, G. D., Prasad, A. A., Jean-Richard-dit-Bressel, P., Yau, J. O. Y., Millan, E. Z., Liu, Y., *et al.*, (2018). Distinct accumbens shell output pathways promote versus prevent relapse to alcohol seeking. *Neuron*, 98(3), 512–520, e516. <https://doi.org/10.1016/j.neuron.2018.03.033>

Gokce, O., Stanley, G. M., Treutlein, B., Neff, N. F., Camp, J. G., Malenka, R. C., *et al.*, (2016). Cellular taxonomy of the mouse striatum as revealed by single-cell RNA-Seq. *Cell Reports*, 16(4), 1126–1137. <https://doi.org/10.1016/j.celrep.2016.06.059>

Groenewegen, H. J., Berendse, H. W., & Haber, S. N. (1993). Organization of the output of the ventral striatopallidal system in the rat: ventral pallidal efferents. *Neuroscience*, 57(1), 113–142. [https://doi.org/10.1016/0306-4522\(93\)90115-v](https://doi.org/10.1016/0306-4522(93)90115-v)

Guerra-Ruiz, J., Navarro, V. I., Negishi, K., & Khan, A. M. (2021). Standardized mapping and high spatial-resolution analysis of the inputs and outputs of the accumbens nucleus “hedonic hotspot” in the male rat using *Brain Maps 4.0*. Presented at the Annual Meeting of the Society for Neuroscience. Online, Nov 8–11.

Guilhemsang, L., & Mallet, N. P. (2024). Arky pallidal neurons in basal ganglia circuits: Unveiling novel pallidostriatal loops? *Current Opinion in Neurobiology*, 84, 102814. <https://doi.org/10.1016/j.conb.2023.102814>

Gurdjian, E. S. (1925). Olfactory connections in the albino rat, with special reference to the stria medullaris and the anterior commissure. *The Journal of Comparative Neurology*, 38, 127–163. <https://doi.org/10.1002/cne.900380202>

Gurdjian, E. S. (1928). The corpus striatum of the rat. *The Journal of Comparative Neurology*, 45, 249–281. <https://doi.org/10.1002/cne.900450110>

Hahn, J. D., Gao, L., Boesen, T., Gou, L., Hintiryan, H., & Dong, H. W. (2022). Macroscale connections of the mouse lateral preoptic area and anterior lateral hypothalamic area. *The Journal of Comparative Neurology*, 530(13), 2254–2285. <https://doi.org/10.1002/cne.25331>

Hahn, J. D., & Swanson, L. W. (2010). Distinct patterns of neuronal inputs and outputs of the juxtapaaraventricular and supraformical regions of the lateral hypothalamic area in the male rat.

Brain Research Reviews, 64(1), 14–103. <https://doi.org/10.1016/j.brainresrev.2010.02.002>

Hahn, J. D., & Swanson, L. W. (2012). Connections of the lateral hypothalamic area juxtadorsomedial region in the male rat. *The Journal of Comparative Neurology*, 520(9), 1831–1890. <https://doi.org/10.1002/cne.23064>

He, J., Kleyman, M., Chen, J., Alikaya, A., Rothenhoefer, K. M., Ozturk, B. E., *et al.*, (2021). Transcriptional and anatomical diversity of medium spiny neurons in the primate striatum. *Current Biology*, 31(24), 5473–5486, e5476. <https://doi.org/10.1016/j.cub.2021.10.015>

Heimer, L., Zahm, D. S., Churchill, L., Kalivas, P. W., & Wohltmann, C. (1991). Specificity in the projection patterns of accumbal core and shell in the rat. *Neuroscience*, 41(1), 89–125. [https://doi.org/10.1016/0306-4522\(91\)90202-y](https://doi.org/10.1016/0306-4522(91)90202-y)

Heimer, L. & Wilson, R. D. (1975). The subcortical projections of the allocortex: similarities in the neural associations of the hippocampus, the piriform cortex, and the neocortex. In: Santini, M. (Ed.) *Golgi Centennial Symposium Proceedings* (Raven Press, New York), pp. 177–193.

Hintiryan, H., Foster, N. N., Bowman, I., Bay, M., Song, M. Y., Gou, L., *et al.*, (2016). The mouse cortico-striatal projectome. *Nature Neuroscience*, 19(8), 1100–1114. <https://doi.org/10.1038/nn.4332>

Hoover, W. B., & Vertes, R. P. (2007). Anatomical analysis of afferent projections to the medial prefrontal cortex in the rat. *Brain Structure and Function*, 212(2), 149–179. <https://doi.org/10.1007/s00429-007-0150-4>

Hueske, E., Stine, C., Yoshida, T., Crittenden, J. R., Gupta, A., Johnson, J. C., *et al.*, (2024). Developmental and adult striatal patterning of nociceptin ligand marks striosomal population with direct dopamine projections. *The Journal of Comparative Neurology*, 532(12), e70003. <https://doi.org/10.1002/cne.70003>

Jay, T. M., & Witter, M. P. (1991). Distribution of hippocampal CA1 and subicular efferents in the prefrontal cortex of the rat studied by means of anterograde transport of *Phaseolus vulgaris*-leucoagglutinin. *The Journal of Comparative Neurology*, 313(4), 574–586. <https://doi.org/10.1002/cne.903130404>

Johnston, J. B. (1923). Further contributions to the study of the evolution of the forebrain. *The Journal of Comparative Neurology*, 35, 337–481. <https://doi.org/10.1002/cne.900350502>

Kelley, A. E., Baldo, B. A., & Pratt, W. E. (2005). A proposed hypothalamic-thalamic-striatal axis for the integration of energy balance, arousal, and food reward. *The Journal of Comparative Neurology*, 493(1), 72–85. <https://doi.org/10.1002/cne.20769>

Khan, A. M. (2013). Controlling feeding behavior by chemical or gene-directed targeting in the brain: What's so spatial about our methods? *Frontiers in Neuroscience*, 7, 1–49. <http://dx.doi.org/10.3389/fnins.2013.00182>

Krettek, J.E. & Price, J. L. (1977). The cortical projections of the mediodorsal nucleus and adjacent thalamic nuclei in the rat. *The Journal of Comparative Neurology*, 171, 157–192. <https://doi.org/10.1002/cne.900170109>

[org/10.1002/cne.901710204](https://doi.org/10.1002/cne.901710204)

Krettek, J. E. & Price, J. L. (1978). A description of the amygdaloid complex in the rat and cat with observations on intra-amygdaloid axonal connections. *The Journal of Comparative Neurology*, 178, 255–280. <https://doi.org/10.1002/cne.901780205>

Kupchik, Y. M., Brown, R. M., Heinsbroek, J. A., Lobo, M. K., Schwartz, D. J., & Kalivas, P. W. (2015). Coding the direct/indirect pathways by D1 and D2 receptors is not valid for accumbens projections. *Nature Neuroscience*, 18(9), 1230–1232. <https://doi.org/10.1038/nn.4068>

Lee, A. T., Vogt, D., Rubenstein, J. L., & Sohal, V. S. (2014). A class of GABAergic neurons in the prefrontal cortex sends long-range projections to the nucleus accumbens and elicits acute avoidance behavior. *The Journal of Neuroscience*, 34(35), 11519–11525. <https://doi.org/10.1523/JNEUROSCI.1157-14.2014>

Lee, J., Wang, W., & Sabatini, B. L. (2020). Anatomically segregated basal ganglia pathways allow parallel behavioral modulation. *Nature Neuroscience*, 23(11), 1388–1398. <https://doi.org/10.1038/s41593-020-00712-5>

Li, S., & Kirouac, G. J. (2008). Projections from the paraventricular nucleus of the thalamus to the forebrain, with special emphasis on the extended amygdala. *The Journal of Comparative Neurology*, 506(2), 263–287. <https://doi.org/10.1002/cne.21502>

Li, S., & Kirouac, G. J. (2012). Sources of inputs to the anterior and posterior aspects of the paraventricular nucleus of the thalamus. *Brain Structure and Function*, 217(2), 257–273. <https://doi.org/10.1007/s00429-011-0360-7>

Li, S., Shi, Y., & Kirouac, G. J. (2014). The hypothalamus and periaqueductal gray are the sources of dopamine fibers in the paraventricular nucleus of the thalamus in the rat. *Frontiers in Neuroanatomy*, 8, 136. <https://doi.org/10.3389/fnana.2014.00136>

Likhtik, E., Stujenske, J. M., Topiwala, M. A., Harris, A. Z., & Gordon, J. A. (2014). Prefrontal entrainment of amygdala activity signals safety in learned fear and innate anxiety. *Nature Neuroscience*, 17(1), 106–113. <https://doi.org/10.1038/nn.3582>

Lorente de Nó, R. (1934). Studies on the structure of the cerebral cortex. II. Continuation of the study of the ammonic system. *Journal für Psychologie und Neurologie*, 46, 113–177.

Luppi, P. H., Fort, P., & Jouviet, M. (1990). Iontophoretic application of unconjugated cholera toxin B subunit (CTb) combined with immunohistochemistry of neurochemical substances: a method for transmitter identification of retrogradely labeled neurons. *Brain Research*, 534(1–2), 209–224. [https://doi.org/10.1016/0006-8993\(90\)90131-t](https://doi.org/10.1016/0006-8993(90)90131-t)

Maldonado-Irizarry, C. S., Swanson, C. J., & Kelley, A. E. (1995). Glutamate receptors in the nucleus accumbens shell control feeding behavior via the lateral hypothalamus. *The Journal of Neuroscience*, 15(10), 6779–6788. <https://doi.org/10.1523/JNEUROSCI.15-10-06779.1995>

Marchant, N. J., Campbell, E. J., Pelloux, Y., Bossert, J. M., & Shaham, Y. (2019). Context-induced relapse after extinction versus punishment: similarities and differences. *Psychopharmacology*

(Berlin), 236(1), 439–448. <https://doi.org/10.1007/s00213-018-4929-1>

McDonald, A. J. (1982). Cytoarchitecture of the central amygdaloid nucleus of the rat. *The Journal of Comparative Neurology*, 208, 401–418. <https://doi.org/10.1002/cne.902080409>

McKenna, J. T., & Vertes, R. P. (2004). Afferent projections to nucleus reuniens of the thalamus. *The Journal of Comparative Neurology*, 480(2), 115–142. <https://doi.org/10.1002/cne.20342>

McNally, G. P. (2021). Motivational competition and the paraventricular thalamus. *Neuroscience and Biobehavioral Reviews*, 125, 193–207. <https://doi.org/10.1016/j.neubiorev.2021.02.021>

Mena, J. D., Sadeghian, K., & Baldo, B. A. (2011). Induction of hyperphagia and carbohydrate intake by mu-opioid receptor stimulation in circumscribed regions of frontal cortex. *The Journal of Neuroscience*, 31(9), 3249–3260. <https://doi.org/10.1523/JNEUROSCI.2050-10.2011>

Mena, J. D., Selleck, R. A., & Baldo, B. A. (2013). Mu-opioid stimulation in rat prefrontal cortex engages hypothalamic orexin/hypocretin-containing neurons, and reveals dissociable roles of nucleus accumbens and hypothalamus in cortically driven feeding. *The Journal of Neuroscience*, 33(47), 18540–18552. <https://doi.org/10.1523/JNEUROSCI.3323-12.2013>

Millan, E. Z., Ong, Z., & McNally, G. P. (2017). Paraventricular thalamus: Gateway to feeding, appetitive motivation, and drug addiction. *Progress in Brain Research*, 235, 113–137. <https://doi.org/10.1016/bs.pbr.2017.07.006>

Mogenson, G. J., Swanson, L. W., & Wu, M. (1983). Neural projections from nucleus accumbens to globus pallidus, substantia innominata, and lateral preoptic-lateral hypothalamic area: an anatomical and electrophysiological investigation in the rat. *The Journal of Neuroscience*, 3(1), 189–202. <https://doi.org/10.1523/JNEUROSCI.03-01-00189.1983>

Morales, I., & Berridge, K. C. (2020). ‘Liking’ and ‘wanting’ in eating and food reward: Brain mechanisms and clinical implications. *Physiology & Behavior*, 227, 113152. <https://doi.org/10.1016/j.physbeh.2020.113152>

Negishi, K., Navarro, V. I., Guerra-Ruiz, J., Sotelo, D., Toccoli, A., & Khan, A. M. (2022). A topographically-defined cortico-striato-pallidal module with convergent projections to the lateral hypothalamic area. Presented at the Annual Meeting of the Society for Neuroscience, San Diego, CA, Nov 12–16. [Program No. 727.11; Nov 16].

Negishi, K., Navarro, V. I., Soto Arzate, L., Guerra Ruiz, J. M., Sotelo, D., Toccoli, A., Khan, A. M. (2023). A topographically-defined hypothalamic-thalamic-striatopallidal connectional motif that supports hedonic processes. Presented at the Annual Meeting of the Society for Neuroscience held Nov 11–15 in Washington, D. C. [PSTR287.21, Nov 13].

Negishi, K., Montes, L. P., Navarro, V. I., Soto Arzate, L., Oliveros, C., & Khan, A. M. (2024). Topographic organization of bidirectional connections between the cingulate region (infralimbic area and anterior cingulate area, dorsal part) and the interbrain (diencephalon) of the adult male rat. *bioRxiv*, 2024.2009.2029.615708. <https://doi.org/10.1101/2024.09.29.615708>

Nissl, F. (1913). Die grosshirnanteile des kaninchens. *Archiv für Psychiatrie und Nervenkrankheiten*,

52, 867–953. <https://doi.org/10.1007/BF02160485>

O'Connor, E. C., Kremer, Y., Lefort, S., Harada, M., Pascoli, V., Rohner, C., & Luscher, C. (2015). Accumbal D1R neurons projecting to lateral hypothalamus authorize feeding. *Neuron*, 88(3), 553–564. <https://doi.org/10.1016/j.neuron.2015.09.038>

Parker, K. E., McCabe, M. P., Johns, H. W., Lund, D. K., Odu, F., Sharma, R., *et al.*, (2015). Neural activation patterns underlying basolateral amygdala influence on intra-accumbens opioid-driven consummatory versus appetitive high-fat feeding behaviors in the rat. *Behavioral Neuroscience*, 129(6), 812–821. <https://doi.org/10.1037/bne0000095>

Paxinos, G., & Watson, C. (2014). *The rat brain in stereotaxic coordinates, 7th edition*. Elsevier/Academic Press.

Peciña, S., & Berridge, K. C. (2005). Hedonic hot spot in nucleus accumbens shell: where do mu-opioids cause increased hedonic impact of sweetness? *The Journal of Neuroscience*, 25(50), 11777–11786. <https://doi.org/10.1523/JNEUROSCI.2329-05.2005>

Petrovich, G. D., Risold, P. Y., & Swanson, L. W. (1996). Organization of projections from the basomedial nucleus of the amygdala: a PHAL study in the rat. *The Journal of Comparative Neurology*, 374(3), 387–420. [https://doi.org/10.1002/\(SICI\)1096-9861\(19961021\)374:3<387::AID-CNE6>3.0.CO;2-Y](https://doi.org/10.1002/(SICI)1096-9861(19961021)374:3<387::AID-CNE6>3.0.CO;2-Y)

Petrovich, G. D., Ross, C. A., Holland, P. C., & Gallagher, M. (2007). Medial prefrontal cortex is necessary for an appetitive contextual conditioned stimulus to promote eating in sated rats. *The Journal of Neuroscience*, 27(24), 6436–6441. <https://doi.org/10.1523/JNEUROSCI.5001-06.2007>

Petrovich, G. D., Setlow, B., Holland, P. C., & Gallagher, M. (2002). Amygdalo-hypothalamic circuit allows learned cues to override satiety and promote eating. *The Journal of Neuroscience*, 22(19), 8748–8753. <https://doi.org/10.1523/JNEUROSCI.22-19-08748.2002>

Prasad, A. A., Xie, C., Chaichim, C., Nguyen, J. H., McClusky, H. E., Killcross, S., *et al.*, (2020). Complementary roles for ventral pallidum cell types and their projections in relapse. *The Journal of Neuroscience*, 40(4), 880–893. <https://doi.org/10.1523/JNEUROSCI.0262-19.2019>

Reppucci, C. J., & Petrovich, G. D. (2016). Organization of connections between the amygdala, medial prefrontal cortex, and lateral hypothalamus: a single and double retrograde tracing study in rats. *Brain Structure and Function*, 221(6), 2937–2962. <https://doi.org/10.1007/s00429-015-1081-0>

Reynolds, S. M., & Berridge, K. C. (2001). Fear and feeding in the nucleus accumbens shell: rostrocaudal segregation of GABA-elicited defensive behavior versus eating behavior. *The Journal of Neuroscience*, 21(9), 3261–3270. <https://doi.org/10.1523/JNEUROSCI.21-09-03261.2001>

Reynolds, S. M., & Berridge, K. C. (2002). Positive and negative motivation in nucleus accumbens shell: bivalent rostrocaudal gradients for GABA-elicited eating, taste “liking”/“disliking” reactions, place preference/avoidance, and fear. *The Journal of Neuroscience*, 22(16), 7308–7320. <https://doi.org/10.1523/JNEUROSCI.22-16-07308.2002>

- Rioch, D. M. (1929). Studies on the diencephalon of Carnivora. Part II: Certain nuclear configurations and fiber connections of the subthalamus and midbrain of the dog and cat. *The Journal of Comparative Neurology*, 49, 121–153. <https://doi.org/10.1002/cne.900490103>
- Risold, P. Y. & Swanson, L. W. (1996). Structural evidence for functional domains in the rat hippocampus. *Science*, 272, 1484–1486. <https://doi.org/10.1126/science.272.5267.1484>
- Riva-Posse, P., Crowell, A. L., Wright, K., Waters, A. C., Choi, K., Garlow, S. J., *et al.*, (2020). Rapid antidepressant effects of deep brain stimulation and their relation to surgical protocol. *Biological Psychiatry*, 88(8), e37–e39. <https://doi.org/10.1016/j.biopsych.2020.03.017>
- Rose, J. E. & Woolsey, C. N. (1948). Structure and relations of limbic cortex and anterior thalamic nuclei in rabbit and cat. *The Journal of Comparative Neurology*, 89, 279–347. <https://doi.org/10.1002/cne.900890307>
- Sally, S. L. & Kelly, J. B. (1988). Organization of auditory cortex in the albino rat: sound frequency. *Journal of Neurophysiology*, 59, 1627–1638. <https://doi.org/10.1152/jn.1988.59.5.1627>
- Sano, T. (1910). Beitrag zur vergleichenden Anatomie der Substantia nigra, des Corps Luysii und der Zona incerta. *Monatsschrift für Psychiatrie und Neurologie*, 28, 26–31.
- Saunders, A., Macosko, E. Z., Wysoker, A., Goldman, M., Krienen, F. M., de Rivera, H., *et al.*, (2018). Molecular diversity and specializations among the cells of the adult mouse brain. *Cell*, 174(4), 1015–1030, e1016. <https://doi.org/10.1016/j.cell.2018.07.028>
- Schwalbe, G. (1881). *Lehrbuch der Neurology*. (Besold, Erlangen).
- Simerly, R. B., Swanson, L. W., & Gorski, R. A. (1984). Demonstration of a sexual dimorphism in the distribution of serotonin-immunoreactive fibers in the medial preoptic nucleus of the rat. *The Journal of Comparative Neurology*, 225, 151–166. <https://doi.org/10.1002/cne.902250202>
- Simmons, D.M. & Swanson, L. W. (2008). High resolution paraventricular nucleus serial section model constructed within a traditional rat brain atlas. *Neuroscience Letters*, 438, 85–89. <https://doi.org/10.1016/j.neulet.2008.04.057>
- Simmons, D. M., & Swanson, L. W. (2009). Comparing histological data from different brains: sources of error and strategies for minimizing them. *Brain Research Reviews*, 60(2), 349–367. <https://doi.org/10.1016/j.brainresrev.2009.02.002>
- Smith, G. E. (1919). A preliminary note on the morphology of the corpus striatum and the origin of the neopallium. *Journal of Anatomy*, 53, 271–291. Available online: <https://pmc.ncbi.nlm.nih.gov/articles/PMC1262868/>
- Smith, K. S., & Berridge, K. C. (2005). The ventral pallidum and hedonic reward: neurochemical maps of sucrose “liking” and food intake. *The Journal of Neuroscience*, 25(38), 8637–8649. <https://doi.org/10.1523/JNEUROSCI.1902-05.2005>
- Soto Arzate, L., Quintana, M., Navarro, V. I., Negishi, K., & Khan, A. M. (2023). Comparisons of the inputs and outputs of the anterior subdivisions of the lateral hypothalamic area in the adult male rat using an open-access atlas framework. Presented at the Annual Meeting of the Society for

Neuroscience held Nov 11–15 in Washington, DC. PSTR287.17, 13 Nov.

Stanley, G., Gokce, O., Malenka, R. C., Sudhof, T. C., & Quake, S. R. (2020). Continuous and discrete neuron types of the adult murine striatum. *Neuron*, *105*(4), 688–699, e688. <https://doi.org/10.1016/j.neuron.2019.11.004>

Stratford, T. R. (2005). Activation of feeding-related neural circuitry after unilateral injections of muscimol into the nucleus accumbens shell. *Brain Research*, *1048*(1–2), 241–250. <https://doi.org/10.1016/j.brainres.2005.05.002>

Stratford, T. R., & Kelley, A. E. (1999). Evidence of a functional relationship between the nucleus accumbens shell and lateral hypothalamus subserving the control of feeding behavior. *The Journal of Neuroscience*, *19*(24), 11040–11048. <https://doi.org/10.1523/JNEUROSCI.19-24-11040.1999>

Swanson, L. W. (1982). The projections of the ventral tegmental area and adjacent regions: a combined fluorescent retrograde tracer and immunofluorescence study in the rat. *Brain Research Bulletin*, *9*(1–6), 321–353. [https://doi.org/10.1016/0361-9230\(82\)90145-9](https://doi.org/10.1016/0361-9230(82)90145-9)

Swanson, L. W. (1992). *Brain maps: structure of the rat brain*. Elsevier, Amsterdam.

Swanson, L. W. (1998). *Brain maps: structure of the rat brain. A laboratory guide with printed and electronic templates for data, models and schematics, 2nd edition* [with 2 CD-ROMs] (Elsevier, Amsterdam).

Swanson, L. W. (2000). Cerebral hemisphere regulation of motivated behavior. *Brain Research*, *886*(1–2), 113–164. [https://doi.org/10.1016/s0006-8993\(00\)02905-x](https://doi.org/10.1016/s0006-8993(00)02905-x)

Swanson, L. W. (2004). *Brain maps: structure of the rat brain. A laboratory guide with printed and electronic templates for data, models and schematics, 3rd edition*. Amsterdam: Elsevier, 215 pp. with CD-ROM, *Brain maps: computer graphics files 3.0*.

Swanson, L. W. (2015). *Neuroanatomical terminology: a lexicon of classical origins and historical foundations*. Oxford: Oxford University Press.

Swanson, L. W. (2018). *Brain maps 4.0—Structure of the rat brain: An open access atlas with global nervous system nomenclature ontology and flatmaps*. *The Journal of Comparative Neurology*, *526*(6), 935–943. <https://doi.org/10.1002/cne.24381>

Swanson, L. W. & Cowan, W. M. (1975). Hippocampo-hypothalamic connections: origin in subicular cortex, not Ammon's horn. *Science*, *189*, 303–304. <https://doi.org/10.1126/science.49928>

Swanson, L. W., Hahn, J. D., & Sporns, O. (2024). Neural network architecture of a mammalian brain. *Proceedings of the National Academy of Sciences, USA*, *121*(39), e2413422121. <https://doi.org/10.1073/pnas.2413422121>

Swanson, L. W., & Hof, P. R. (2019). A model for mapping between the human and rodent cerebral cortex. *The Journal of Comparative Neurology*, *527*(17), 2925–2927. <https://doi.org/10.1002/cne.24708>

Tang, H., Bartolo, R., & Averbeck, B. B. (2024). Ventral frontostriatal circuitry mediates the

computation of reinforcement from symbolic gains and losses. *Neuron*, 112(22), 3782–3795, e3785. <https://doi.org/10.1016/j.neuron.2024.08.018>

Tarin, P. (1753). *Dictionnaire Anatomique suivi d'une Bibliotheque Anatomique et Physiologique* (Briasson, Paris).

Thompson, R. H., & Swanson, L. W. (2010). Hypothesis-driven structural connectivity analysis supports network over hierarchical model of brain architecture. *Proceedings of the National Academy of Sciences, USA*, 107(34), 15235–15239. <https://doi.org/10.1073/pnas.1009112107>

Tsai, C. (1925). The optic tracts and centers of the opossum, *Didelphis virginiana*. *The Journal of Comparative Neurology*, 39, 173–216. <https://doi.org/10.1002/cne.900390202>

Varela, C., Kumar, S., Yang, J. Y., & Wilson, M. A. (2014). Anatomical substrates for direct interactions between hippocampus, medial prefrontal cortex, and the thalamic nucleus reuniens. *Brain Structure and Function*, 219(3), 911–929. <https://doi.org/10.1007/s00429-013-0543-5>

Vertes, R. P. (2004). Differential projections of the infralimbic and prelimbic cortex in the rat. *Synapse*, 51(1), 32–58. <https://doi.org/10.1002/syn.10279>

Vertes, R. P., & Hoover, W. B. (2008). Projections of the paraventricular and paratenial nuclei of the dorsal midline thalamus in the rat. *The Journal of Comparative Neurology*, 508(2), 212–237. <https://doi.org/10.1002/cne.21679>

Vertes, R. P., Linley, S. B., & Hoover, W. B. (2015). Limbic circuitry of the midline thalamus. *Neuroscience and Biobehavioral Reviews*, 54, 89–107. <https://doi.org/10.1016/j.neubiorev.2015.01.014>

Vesalius, A. (1543). *De Humani Corporis Fabrica Libri Septem*. (Oporinus, Basel).

Watts, A. G., Kanoski, S. E., Sanchez-Watts, G., & Langhans, W. (2022). The physiological control of eating: signals, neurons, and networks. *Physiological Reviews*, 102(2), 689–813. <https://doi.org/10.1152/physrev.00028.2020>

Watts, A. G., & Swanson, L. W. (2002). Anatomy of Motivation. In *Stevens' Handbook of Experimental Psychology*. <https://doi.org/https://doi.org/10.1002/0471214426.pas0314>

Watts, A. G., Swanson, L. W., & Sanchez-Watts, G. (1987). Efferent projections of the suprachiasmatic nucleus: I. Studies using anterograde transport of *Phaseolus vulgaris* leucoagglutinin in the rat. *The Journal of Comparative Neurology*, 258, 204–229. <https://doi.org/10.1002/cne.902580204>

Wickersham, I. R., Lyon, D. C., Barnard, R. J., Mori, T., Finke, S., Conzelmann, K. K., et al., (2007). Monosynaptic restriction of transsynaptic tracing from single, genetically targeted neurons. *Neuron*, 53(5), 639–647. <https://doi.org/10.1016/j.neuron.2007.01.033>

Wouterlood, F. G., & Groenewegen, H. J. (1985). Neuroanatomical tracing by use of *Phaseolus vulgaris*-leucoagglutinin (PHA-L): electron microscopy of PHA-L-filled neuronal somata, dendrites, axons and axon terminals. *Brain Research*, 326(1), 188–191. [https://doi.org/10.1016/0006-8993\(85\)91402-7](https://doi.org/10.1016/0006-8993(85)91402-7)

Zahm, D. S., & Heimer, L. (1993). Specificity in the efferent projections of the nucleus accumbens in the rat: comparison of the rostral pole projection patterns with those of the core and shell. *The Journal of Comparative Neurology*, 327(2), 220–232. <https://doi.org/10.1002/cne.903270205>

Ziehen, T. (1897–1901). Das Centralnervensystem der Monotremen und Marsupialier. *Denkschriften der Medicinisch-naturwissenschaftlichen Gesellschaft zu Jena*, 6, 1–187, 677–728.

Zingg, B., Chou, X. L., Zhang, Z. G., Mesik, L., Liang, F., Tao, H. W., & Zhang, L. I. (2017). AAV-mediated anterograde transsynaptic tagging: Mapping corticocollicular input-defined neural pathways for defense behaviors. *Neuron*, 93(1), 33–47. <https://doi.org/10.1016/j.neuron.2016.11.045>

Zingg, B., Peng, B., Huang, J., Tao, H. W., & Zhang, L. I. (2020). Synaptic specificity and application of anterograde transsynaptic AAV for probing neural circuitry. *The Journal of Neuroscience*, 40(16), 3250–3267. <https://doi.org/10.1523/JNEUROSCI.2158-19.2020>